Normal fault growth in layered basaltic rocks: the role of strain rate in fault evolution

A. Bubeck[1], R.J. Walker[1], J. Imber[2], C.J. MacLeod[3]

[1]*School of Geography, Geology, and the Environment, University of Leicester, University Road, Leicester, UK.*

[2]*Department of Earth Sciences, Durham University, Science Labs, Durham, UK.*

[3]*School of Earth and Ocean Science, Cardiff University, Park Place, Cardiff, UK*

[*]*Correspondence (ab753@le.ac.uk)*

ABSTRACT

Conceptual models for the evolution of dilatant faults in volcanic rift settings involve a step-wise growth pattern, involving upward propagation of subsurface faults, surface monocline formation, which are breached by subvertical, open faults. Immature, discontinuous normal faults are considered representative of the early stages of mature, linked faults that accommodate extensional strains. We consider the evolution of surface-breaking normal faults using a comparison of the distribution and geometry of normal faults from two volcanic rift zones: the Koa‘e fault system, Hawai‘i, and the Krafla fissure swarm, NE Iceland. Field mapping highlights similarities to current predicted geometries, but also prominent differences that are not reconciled by current models. Variable deformation styles record magma supply changes within the rift zones, which drive local strain rate gradients. Building on existing studies, we present a conceptual model of fault growth that accounts for spatial and temporal changes in strain rate within the deforming regions. We propose that faults in separate rift systems may not advance through the same stages of evolution and that faults within *individual* rift systems can show differing growth patterns. Variations in

surface strains may be indicative of subsurface magmatic system changes, with important implications for our understanding of volcano-tectonic coupling.

Key words: normal fault; monocline; extension; basalt; volcanic rift

1.1. Introduction

Normal fault systems comprise discontinuous, non-collinear segments, with overlaps and segment linkage commonly resulting in characteristic overlapping or step-like geometries across a broad range of scales (e.g. Segall and Pollard, 1980; Peacock, 2002; Long and Imber, 2011). Regional extension is conserved ahead of first-order fault terminations by areas of folding and linking faults and fractures (e.g. Morley et al., 1990; Faulds and Varga, 1998). The geometry and distribution of structures within these domains play an important role in the tectono-stratigraphic development of rift basins (e.g. Lambiase and Bosworth, 1995; Sharp et al., 2000; Hus et al., 2006), and the evolving fluid flow properties of fault zones (e.g. Manzocchi et al., 2010; Seebeck et al., 2014). Much of our current understanding of the growth of normal fault populations and fault zone architecture is derived from studies of faults in clastic sequences using combinations of: (1) fault analysis and scaling relationships, based on field and seismic data-derived measurements of displacement and length versus width (e.g. Ferrill and Morris, 2001; Peacock, 2002; Walsh et al., 2003; Nixon et al., 2014); (2) scaled-analogue modelling (e.g. Holland et al., 2006; Tentler and Acocella, 2010); and (3) numerical-based modelling techniques (e.g. Crider and Pollard, 1998; Maerten et al., 2002; Schöpfer et al., 2006). Many of these studies have focussed on fault propagation and segmentation within layered clastic sequences (e.g. Ferrill and Morris, 2003), and more recently crystalline-clastic sequences (e.g. Peacock and Parfitt, 2002; Holland et al., 2006; Martel and Langley, 2006; Kaven and Martel, 2007; Walker et al., 2013). The growth of normal

47 faults in layered basaltic sequences, and the expression of those faults outcropping at surface, has
48 become increasingly important in recent years, driven in part by interest in intra- and sub-volcanic
49 hydrocarbon plays along volcanic passive margins (e.g., the NE Atlantic basins: Davison et al.,
50 2004; Walker et al., 2012, 2013), as well as high-temperature shallow geothermal systems that rely
51 on basaltic stratigraphy (e.g. Anderson and Bowers, 1995; Helm-Clark et al., 2004) and models of
52 volcanic flank stability (e.g. Le Corvec and Walter, 2009; Plattner et al., 2013). An improved
53 understanding of basalt-hosted fault zones has important implications for extension in continental
54 and oceanic systems on Earth, as well as on other planets (e.g. Hauber et al., 2010; Vaz et al.,
55 2014).

56 Existing models for the growth of normal faults in basaltic sequences typically depict
57 development in a common series of static stages with the progression between stages treated as
58 instantaneous (e.g. Martel and Langley, 2006). Emphasis is placed on the reactivation of pre-
59 existing cooling joints through the entire layer sequence; considered to be the first-order control
60 on the distribution, geometry and architecture of basalt-hosted fault zones (e.g. Forslund and
61 Gudmundsson, 1992; Gudmundsson, 2011). A single growth process implies that small-
62 displacement faults in immature or early-stage rift systems are also representative of faults in more
63 advanced systems, with all faults progressing through the same stages of evolution. As such,
64 models of fault growth in cohesive sequences are broadly applied to a wide range of settings.

65 Here, we present a detailed field study of the distribution and geometry of well-exposed
66 extensional structures in two developing volcanic rift zones - the Koa‘e fault system, Hawai‘i, and
67 the Krafla fissure swarm, NE Iceland - to compare and contrast evolving segmentation patterns
68 during rift development. Field mapping reveals that surface-breaking faults in separate rift systems
69 can follow different growth pathways during propagation. Faults that are located within *individual*

rift systems can also demonstrate differing growth patterns. Our new observations build on previous observations (e.g. Grant and Kattenhorn, 2004; Holland et al., 2006; Martel and Langley, 2006; Kaven and Martel, 2007), and extend models, conceptually, for fault growth in layered basaltic sequences.

2.1. Background: near-surface faults in layered basaltic sequences

Existing studies of near-surface normal fault development in layered basaltic sequences identify four principal characteristics: (1) sinuous zones of vertical extension fractures (dominantly in the footwall, but also in the hanging wall); (2) monoclinal folding of the ground surface; (3) sub-vertical, surface-breaking fault scarps that show a component of dilation; and (4) less commonly, hanging wall buckles found proximally to the scarp bases (Duffield, 1975; Acocella et al., 2000; Grant and Kattenhorn, 2004; Martel and Langley, 2006; Holland et al., 2006; Villemin and Bergerat, 2013). These characteristics are expected to show predictable geometries, resulting from the following successive stages: (1) nucleation of a normal fault at depth; (2) slip on the fault at depth drives both folding of the free surface into a monocline, and tensile stress concentrations that result in the opening of pre-existing cooling joints in the footwall ahead of the fault tip; (3) with continued slip and upward propagation, the monocline becomes steeper and narrower, and footwall fractures widen and propagate downwards; (4) eventual linkage of surface extension fractures with fault tips at depth leads to systematic breaching of surface monoclines and the development of sub-vertical, surface-breaking fault segments that display horizontal and vertical components of displacement. Previous work has also invoked a downward fault growth model to account for fault patterns in basaltic sequences (e.g. Opheim and Gudmundsson, 1989). Here, we focus on the upward propagation model, which is more strongly supported by existing field

93 observations and numerical models (e.g. Grant and Kattenhorn, 2004; Martel and Langley, 2006;
94 Kaven and Martel, 2007).

95 Based on upward growth models, we might expect predicted geometries (i.e. monoclinal
96 folding of basaltic layering) to be preserved at depth following upward propagation of blind normal
97 faults (e.g. Holland et al., 2006). Notably, field studies of exhumed basaltic fault zones have found
98 little evidence for folding, implying that they may not represent precursory features of all basalt-
99 hosted normal faults (e.g. Walker et al., 2012, 2013).

100 To date, an upward growth model has been broadly applied to normal fault growth in
101 cohesive sequences for a range of geological settings on Earth, including the Koa‘e fault system,
102 Hawai‘i (e.g. Holland et al., 2006; Podolsky and Roberts, 2008), Iceland (e.g. Grant and
103 Kattenhorn, 2004; Villemin and Bergerat, 2013), the East Africa Rift (e.g. Casey et al., 2006;
104 Rowland et al., 2007), mid ocean ridges (e.g. Soule et al., 2009; Escartin et al., 2016), and on other
105 planets, including: Mars (e.g. Caparelli et al., 2007; Tanaka et al., 2008; Schultz et al., 2010),
106 Enceladus (e.g. Nahm and Kattenhorn, 2015) and Earth’s Moon (e.g. Nahm and Schultz, 2015).
107 Most of the models derived for these systems involve a deforming volume that is mechanically
108 isotropic, and undergoes uniformly applied boundary stresses at a constant strain rate. Using
109 detailed field observations of surface structures in the Koa‘e fault system, Hawai‘i and the Krafla
110 fissure swarm in northern Iceland, we build upon the existing field-data-constrained numerical
111 models of Martel and Langley (2006) and demonstrate that there is an inherently four-dimensional
112 distribution of extensional strains and strain rates within developing volcanic rift zones. Our aim
113 is to show that the evolving first-order geometry and distribution of normal faults is sensitive to
114 variations in boundary stress conditions and the mechanical properties of the deforming sequence.
115

2.2. Methods

Surface structures in the Koa'e and Krafla fault systems were mapped using a combination of high resolution aerial images (GoogleEarth™ and World-View2: 0.5 m resolution), topographic datasets (aerial LiDAR: 0.5 m resolution (Koa'e only)), and traditional field mapping techniques. At the free surface, in both study areas, extension fractures (hereafter, *fractures*) appear to have initiated along pre-existing cooling joints in the lava pile, producing characteristic zigzag trace geometries (Figure 1). This is consistent with geometries that have previously been identified (e.g. Grant and Kattenhorn, 2004; Martel and Langley, 2006; Villemin and Bergerat, 2013).

FIGURE 1 HERE

This zig-zag geometry presents multiple piercing points in plan view, allowing displaced walls to be matched across the open fracture aperture (less than ~3 m; beyond this width, erosion and collapse can alter the fracture profile), and hence, accurate measurement of the following (see Figure 1): (1) extension direction and mode (extension, mode-I; extensional-shear, mixed-mode); (2) the amount of horizontal opening across the fracture, here referred to as fracture aperture; (3) fracture trace azimuth, equivalent to the strike of the fault plane; and (4) vertical offset of the free surface, where present. Remote and field data are combined to characterise the distribution, and geometry of fractures and surface-breaking normal faults, as well as monocline distribution, extent, and geometry to sub-metre precision and accuracy.

3. Surface-breaking fault systems in volcanic rift zones

3.1. Early stage rift development: The Koa'e fault system, Hawai'i

139 The Koa‘e fault system borders the south flank of Kīlauea Volcano (Figure 2A), which is the
140 youngest and southernmost subaerial volcano in the Hawaiian-Emperor chain, and one of five
141 volcanic systems on the Island of Hawai‘i (Neal and Lockwood, 2003). Melting, generated by an
142 upwelling mantle plume, impinges on the lithosphere, through which magma ascends via a system
143 of conduits into a series of interconnected shallow storage reservoirs at ~2.5-4 km and at ~2 km
144 depth beneath Kīlauea ’s summit (e.g. Baker and Amelung, 2012; Lin et al., 2014). Repeated influx
145 of magma into these storage reservoirs, at rates of ~0.1 $km^3\ y^{-1}$ (Swanson et al., 1976; Dzurisin et
146 al., 1984; Poland et al., 2014), typically results in episodes of inflation and deflation, driving
147 eruptive episodes either at the summit, or shallow intrusion and eruption within two pronounced
148 rift zones: the Southwest and East Rift Zones (Figure 2A,B), which radiate south-westward and
149 eastward from the summit (Duffield et al., 1982; Wright and Klein, 2006; Poland et al., 2012).
150 Records of sustained eruptions at Kīlauea ’s summit show that the duration and volume of magma
151 associated with eruptive episodes can vary significantly: In June 1952, 38 x 10^6 m^3 of magma was
152 erupted over 136 days and in November 1967, 64 x 10^6 m^3 of magma was erupted over 251 days.
153 Between 1983-2003, Kīlauea was in a phase of continuous eruption with ~200 x 10^6 m^3 of magma
154 released (Dvorak and Dzurisin, 1993; Poland et al., 2012). As a result of complex dynamics of the
155 system, extension rates across Kīlauea also vary considerably from: ~26 cm/y^{-1} between 1975-
156 1983 to <5 cm/y^{-1} since 1983 (Delaney et al., 1990, 1998). Flank displacement is linked to periods
157 of shallow intrusion within the rift zones and summit region, and/or periods of gravitational sliding
158 on a basal detachment at a depth of approximately 9 km (e.g. Klein et al., 1987; Delaney et al.,
159 1990; Denlinger and Okubo, 1995; Le Corvec and Walter, 2009).
160
161 *FIGURE 2 HERE*

Our study area is within the Koa‘e fault system, which is a 12 km long, ~3 km wide zone of normal faulting (Figure 2A), that connects the Southwest and East Rift Zones (SWRZ and ERZ, hereafter) to form a continuous, 60-70 km long, ENE-WSW trending zone of extension. Normal faults in the system are growth faults, interpreted to be related both to the forceful emplacement of dykes into the rift zones of Kīlauea Volcano (Duffield et al., 1975, 1982; Swanson et al 1976; Peacock and Parfitt, 2002) and to gravitationally induced volcano spreading (Poland et al., 2014 and references therein). The area is characterized by small-volume tholeiitic pahoehoe type lavas, emplaced as inflated sheets, onto the subhorizontal (1-2°) volcano flank. Individual lava thickness is highly variable. Cross-sectional views, normal to the lava flow direction, show maximum thicknesses of up to 4 m (e.g., Hon et al., 1994; Bubeck et al., 2017a), but taper laterally to tens-of-centimetre thicknesses at the tens-of-metre to hundred-metre length scales.

3.1.1. Surface structures in the Koa‘e fault system

Mapping in the Koa‘e fault system reveals three characteristic structures (Figure 2B): (1) ENE-WSW striking (ERZ-parallel) faults, with sub-vertical NNW-dipping scarps that show maximum throws of 12-16 m; (2) fracture networks that are grouped into two orientations: ENE-WSW (ERZ-parallel) and NW-SE (ERZ-oblique); and (3) N to NNW-dipping monoclinal folds, which are discontinuous, show variable amplitudes of up to 12 m, and have crests that are parallel to the strike of major normal faults and the strike of the ERZ. ENE-WSW striking fractures dominate in the Koa`e whereas NW-SE striking fracture sets form obliquely oriented steps along fracture (cm-10s of m scale) and fault (hundreds of metre, to km scale) traces (Bubeck et al., 2017b). An additional feature located in the immediate hanging wall of some faults are localized buckle

185 structures with anticlinal crests that parallel the strike of the ERZ and show amplitudes of up to 2
186 m.

187 Fracture networks form sinuous zones up to ~5 km in length and 30-50 m wide (Figure
188 3A). Most of these zones are limited to the footwalls of surface-breaking normal faults and along
189 the upper limb of monoclines, where they parallel the strike of the fold crest. Less commonly,
190 fractures are found in the hanging walls of faults, and as isolated zones in areas of the fault system
191 where fault scarps are absent and there is no evidence for monoclinal flexure of the surface (Figure
192 3B, C; Figure 4A).

193

194 *FIGURE 3 HERE*

195 A summary of orientation and kinematic data for fractures and normal faults are presented here;
196 more detailed orientation, aperture and kinematic data are presented in Bubeck et al. (2017b).
197 Zones of rift-parallel (ENE-WSW) fractures are most common (~85% of mapped traces) and show
198 individual fracture trace lengths of up to ~370 m. Apertures may be as much as ~4 m, but are more
199 commonly in the range of 0.3-0.6 m (Bubeck et al., 2017b). NW-SE striking fracture zones are
200 less common (~15% of mapped traces) with individual fracture trace lengths of ~4-120 m and
201 apertures of 0.02-2.50 m (Bubeck et al., 2017b). Field characterization of fractures in the study
202 identified only extensional openings (i.e. orthogonal to fracture azimuth; e.g. Figure 1) and we
203 recorded no preferred stepping direction between segmented fracture traces. NW-SE striking
204 fractures tend to occur in close association with the lateral terminations of rift-parallel normal
205 faults and footwall fractures, occurring as obliquely oriented steps or linkages between segments
206 (Figure 2B; Bubeck et al., 2017b). Individual fractures that outcrop for >10 m (e.g. Figure 3A, B;
207 Figure 4) in the study area commonly display multiple steps along their length in plan view,

suggesting they represent composite fractures produced by linkage of segments (e.g. Peacock and Sanderson, 1991). At the scale of the individual fractures (i.e. beyond the scale of joint-related irregularities), shorter fractures (<10 m in length) also display non-linear traces with obliquely oriented steps, hook-shaped tips, or abutting geometries in the vicinity of neighboring structures (Figure 3C). Fractures of this length scale are most commonly found along the upper limbs of monoclines where they form distributed networks (Figure 3A, 4B). In some instances, these networks are set back from the region of present day maximum curvature (Figure 4B) and elsewhere they follow regions of maximum curvature on monocline limbs (Figure 4C).

FIGURE 4 HERE

Monoclinal folds in the Koa'e fault system may be divided into two scales: (1) monoclines that are laterally continuous at the kilometre scale, for distances up to 3 km (Figure 2B, 5A); and (2) monoclines that are laterally discontinuous, with maximum lengths of ~150 m (Figure 2B, 5B). Continuous monoclines are observed in the western and central-western areas of the fault system (Figure 2B); folds show rounded morphologies with amplitudes of up to ~16 m (Figure 5A, 6A-C) and limbs dip gently (typically ~15º but, locally up to ~25 º) (Figure 6D, 7A).

FIGURE 5 HERE

This is in agreement with the models of Martel and Langley (2006) and Kaven and Martel (2007) who predicted monoclines will steepen as faults approach the free surface. Such patterns were also recorded by Podolsky and Roberts (2008) along the White Rabbit Fault (Figure 2b); these authors,

however, instead linked along-strike variations in monocline amplitude to local occurrence of relay ramps ahead of the tips of previously soft-linked segments, rather than to upward propagation-related folding.

FIGURE 6 HERE

Such fault tip monoclines are particularly clear along the Ohale Pali (Figure 2B) where discontinuous folds occur as isolated lenses caught between en echelon fault segments (Figure 7B). The monoclines described in this study, however, are distinct from this relay ramp tilting mechanism.

Discontinuous monoclines are restricted to the eastern region of the Koa'e fault system, and are most common along the Kulanaokuaiki Fault (Figure 2B) where they form isolated, often disintegrated blocks with maximum amplitudes of up to ~15 m in the centre of each block, decreasing steeply (~30º) to zero at the lateral tips (Figure 5B, 7C). Breached examples were not observed. The hanging wall free surface that is offset across adjacent fault scarps is relatively planar. The width of the folded limb of these structures does not vary greatly, ranging from 10 to 20 m. These monoclines feature large (often >4 m wide) composite fractures along their upper limb and tend to be connected laterally with large, open fault scarps with vertical offsets up to 12 m. Monoclines of this type are decoupled from the footwall along these continuous co-linear composite extension fractures (Figure 5B, 7C). The limited lateral extent of the short monoclines, fragmented appearance, and localised steep dip are consistent with a fault-bound block rotation of the immediate hanging wall, effected by blind antithetic faults rather than a monoclinal fold. Such

253 rotational features have been produced in analogue models of fault propagation in brittle sequences
254 (e.g. Holland et al., 2006; Michie et al., 2014).
255
256 *FIGURE 7 HERE*
257
258 Where present, neither type of monocline has been systematically breached, despite being
259 parallel to the strike of prominent normal faults in the region (Figure 2B). Where breaching has
260 been observed, vertical offsets on the monocline-breaching segments are minor (up to 6 m) (Figure
261 6B) compared to collinear fault scarps (up to 16 m throw) (Figure 8).
262 Where present, sub-vertical normal faults in the area typically offset the surface by up to
263 ~15 m (Figure 5B, Figure 7). In addition to a vertical component of displacement, all surface-
264 breaking fault segments exhibit horizontal openings along composite fracture traces with apertures
265 of up to ~5 m. Fault scarps preserve cooling joint-related irregularities (e.g. Figure 1) and we find
266 no evidence for slickenlines or slickensides on fracture surfaces to indicate initial shear
267 displacement, consistent with observations in previous studies (e.g. Holland et al., 2006; Peacock
268 and Parfitt, 2002).
269
270 *FIGURE 8 HERE*
271
272 It is not possible to determine from field study alone whether fault slip at depth was purely
273 dip-slip. Seismicity records suggest that strike-slip and oblique-slip faulting is common at depths
274 of 0.5-5.0 km below the Koa‘e fault system (Lin and Okubo, 2016), but the surface expression of
275 this on the mapped faults is unclear. Mapping has revealed that surface-breaking normal fault

276 segments (up to 200 m in length) are most commonly found in the central-eastern and eastern
277 regions of the fault system, within ~5 km of the upper ERZ. Based on the total lengths of
278 deformation zones (up to 5 km; Figure 2B), our interpretation of these segments is that they
279 represent discontinuous splays of single fault structures at depth. Based on remote mapping
280 techniques, surface-breaking fault segments that offset planar footwall and hanging wall surfaces
281 are estimated to comprise approximately 20% of inferred fault traces in the Koa‘e fault system;
282 the remaining ~80% is characterised by monoclinal folding, blind normal faults, and rarely,
283 monocline-breaching fault segments.
284
285 **3.2. Advanced stage rift development: The Krafla fissure swarm, Iceland**
286 Iceland is located on the plate boundary between North America and Eurasia, and represents a
287 subaerially exposed segment of the Mid-Atlantic Ridge. The Icelandic axial rift zone (the Neo-
288 Volcanic Zone: NVZ) accommodates WNW-ESE (104°) extension of ~19 mm/year (e.g.
289 Sæmundsson, 1974; Wright et al., 2012) across 5 sub-parallel NNE-SSW-striking en echelon
290 volcanic systems and associated fissure swarms: Theistareykir, Krafla, Fremri-Namur, Askja, and
291 Kverkfjöll (Figure 8A). Extension in these zones is accommodated by systems of normal faults,
292 sub-parallel eruptive fissures, and extension fractures that radiate outward from axial volcanoes in
293 a direction orthogonal to the regional minimum horizontal stress (e.g. Sæmundsson, 1974;
294 Brandsdóttir and Einarsson, 1979). The Krafla central volcano and associated fault and fracture
295 networks have dominated volcanic activity in the axial rift zone, with approximately 35 Holocene
296 basaltic eruptions identified (Brandsdóttir and Einarsson, 1979; Opheim and Gudmundsson,
297 1989). The rift zone extends 80-100 km along strike (Figure 9A), with a width of 4-10 km
298 (Bjornsson et al., 2007).

299 Magma is stored beneath the central volcano, in a reservoir at approximately 2.5-3.0 km
300 depth and supplied at a rate of ~1.6 km^3 per year (Tryggvason, 1986; Dauteuil et al., 2001). Records
301 of ground deformation, dating back to 1976, highlight pronounced and repeated episodes of steady
302 inflation followed by rapid deflation (and subsidence), associated with rift zone extension
303 (Bjornsson et al., 1978; Tryggvason, 1984; Rubin, 1992). The scale and duration of these episodes
304 is highly variable. For instance, 30-40 x 10^6 m^3 was erupted from Krafla in 1980 over a period of
305 12 hours. In another episode deflation of the summit reservoir released 198 x 10^6 m^3 over 39 days.
306 During those events, large portions of the rift zone are known to have extended: between 1974-78,
307 up to eight separate inflation-deflation events were recorded and 80-90 km of the ~100 km long
308 rift zone accommodated extension (Tryggvason, 1984). Lateral dyke propagation has been
309 recorded for large distances (~50 km) along the rift zone (Bjornsson et al., 1978; Buck et al., 2006;
310 Hjartardóttir et al., 2012). Based on the ages for lava flows and erosional surfaces, deformation
311 rates are estimated to be between 1.5-15 cm/y^{-1} (Dauteuil et al., 2001). Lavas in the study area
312 dominantly are of pahoehoe type, with individual unit thickness ranging from ~10 cm, up to ~3 m.
313 Lava thicknesses in the study area are reasonably constant (+/- 10%) over the hundred-metre length
314 scale.
315
316 *FIGURE 9 HERE*
317
318 **3.2.1. Surface structures in the Krafla fissure swarm**
319 Here we focus on an area of the Krafla rift system ~10 km north of Krafla Volcano (Figure 9B,
320 C). Detailed measurements of orientation, kinematics and aperture of fractures and normal faults
321 are presented in Bubeck et al. (2017b); here we provide a summary. Mapping reveals the following

322 structures (Figure 9C, D): (1) rift zone-parallel (NNE-SSW strike) normal faults, with sub-vertical
323 scarps that dip to the WNW and ESE, and accommodate displacements >15 m; (2) networks of
324 fractures found dominantly within the footwall (and less commonly in the hanging wall) of
325 surface-breaking normal faults; and (3) rarely, monoclinal folds and hanging wall buckles.
326 Fractures are grouped into three dominant strike orientations (Figure 9D): NNE-SSW (rift-
327 parallel), NW-SE (rift-oblique), and WNW-ESE (rift-normal). Importantly, fractures with
328 orientations outside of the principal rift trend (NNE-SSW) are not randomly distributed but show
329 a close spatial association with the tips of en echelon rift faults (Bubeck et al. 2017b).

330 Fractures in the Krafla fissure swarm form linear zones that are up to 5 km long and 5-15
331 m wide. Rift-parallel striking fractures of this order are most common in the study area (~60% of
332 mapped fracture traces) and show lengths of up to ~800 m, with apertures of up to 4 m, but
333 commonly in the range 1.0-1.5 m (Bubeck et al., 2017b). Rift-oblique (NW-SE) striking fractures
334 are less frequent (~30% of mapped fracture traces), but accommodate similar scales of opening
335 (up to 4 m; modal opening is 2.0-2.5 m) across open fault scarps, with lengths up to ~50 m (Bubeck
336 et al., 2017b). Rift-normal (WNW-ESE) striking fractures are least common (~10% of mapped
337 fracture traces) and show the smallest lengths (less than ~40 m) and apertures (up to ~1 m) (Bubeck
338 et al., 2017b). None of the fracture sets identified show a preferred stepping direction, and
339 individual fractures show prominent obliquely-oriented steps in their traces, which commonly
340 coincide with points of aperture minima. Such patterns have been interpreted previously elsewhere
341 to represent sites of segment linkage between originally segmented structures (e.g. Peacock and
342 Sanderson, 1991). At the scale of whole fractures (tens to hundreds of metre scale), traces are
343 linear and considered composite structures: i.e. they represent coalesced fractures that were
344 originally segmented.

FIGURE 10 HERE

Extension in the Krafla fissure swarm is accommodated dominantly by large (>15 m displacement), sub-vertical surface-breaking faults that offset planar footwall-hanging wall surfaces (Figure 10). Faults are continuous in length for 0.5-1.5 km and parallel to the NNE-SSW trend of the rift zone, accommodating WNW-ESE extension (Figure 9B, D). As observed in the Koa‘e fault system, faults show significant horizontal openings of up to 4 m, in addition to a vertical component of displacement (Figure 9). A sub-set of shorter normal faults (<0.5 km length) and fractures, which strike at a low angle to the main rift trend (i.e. NW-SE), occurs at the terminations of rift-parallel faults (e.g. Figure 9B) (Bubeck et al., 2017b). Fractures in this trend show prominent strike-slip displacements, in addition to open components (Bubeck et al., 2017b). Strike-slip motion has not been observed across NW-SE striking fault segments, however it should be noted that the lack of preserved piercing points precludes documentation of any horizontal component of motion in this case.

Crests of monoclines are parallel to the NNE-SSW trend of the rift zone and strike of normal faults (Figure 9C, 11). Based on their spatial extent, only laterally discontinuous (<50 in length) monoclines are identified. Monoclines in the Krafla fissure swarm typically have low amplitudes (<10 m) and rounded morphologies, with open fractures along the upper limb, which are collinear with adjacent open normal fault scarps on either side of the monocline (Figure 11A). Breached monoclines are more common in the Krafla study area.

FIGURE 11 HERE

Where monoclines are breached, amplitudes are generally low (<2 m) and extensional strains have localised on the breaching fault segment, which in some instances, have accrued throws of 0.5-1.0 m (e.g. Figure 11B). Along one fault segment there is also evidence for multiple monocline geometries with the development of an additional fold further into the hanging wall, ahead of a breached monocline (Figure 11B). Instances of heavily fractured or disintegrated morphologies, though less common in the Krafla study area, show steep rotations of up to 90° (Figure 11C). Importantly, monoclines in the Krafla fissure swarm are comparatively rare and are associated with smaller rift-parallel striking faults (throw <15 m), rather than representing characteristic features of all faults.

4. Discussion

4.1. Comparison of surface structures in the Koa‘e and Krafla fault systems

Field observations of the distribution and geometry of normal faults in the Koa‘e fault system and the Krafla fissure swarm show similar structural features to one another, and to existing predicted geometries (e.g. Grant and Kattenhorn, 2004; Holland et al., 2006; Martel and Langley, 2006; Kaven and Martel, 2007), including: (1) sub-vertical fault scarps with prominent openings (2-4 m); (2) monoclines that strike parallel to rift faults and decrease in width as they increase in height prior to breaching; and (3) zones of sub-vertical fractures that appear to activate pre-existing cooling joints. These shared structural features are predicted to follow a stepwise and systematic evolution with earlier features evident in advanced stages (e.g. Martel and Langley, 2006; Kaven and Martel, 2007).

390 In general, surface-breaking faults in the Krafla fissure swarm are larger (>15 m throw),
391 longer (>500 m) and more prevalent than surface-breaking faults in the Koa‘e. Extension fracture
392 networks in the Koa‘e are more distributed and comprise a greater number of shorter (between 10-
393 20 m) and narrower (typically 0.3-0.6 m aperture) fractures. These characteristics lead us to
394 consider that faults in the Krafla fissure swarm are in a more advanced stage of development, and
395 accommodate greater strains than structures in the Koa‘e fault system. We might therefore expect
396 faults in both settings to follow the same evolutionary path, as has been suggested previously (e.g.,
397 Martel and Langley, 2006), with faults in Krafla to be in a more advanced stage of the same
398 development process.

399 Our field observations, however, highlight prominent departures from both the predicted
400 geometries in the models, and between the two locations; specifically, precursory monoclines are
401 not present along all fault traces, where they ought to be systematically breached. In the Koa‘e
402 fault system, monoclines are not uniformly distributed, but rather they are restricted to central-
403 western and western regions of the fault system (Figure 2B), where they form continuous structural
404 features for up to ~3 km; amplitudes are similar to the surface-breaking fault segments in the
405 eastern portions of the fault system. In the east of the fault system, within ~5 km of the upper ERZ,
406 large (5-15 m throw) surface-breaking faults dominate and outcrop as subvertical scarps with open
407 fractures at their base, with few instances of folding of the ground surface prior to breaching. The
408 result of this distribution of deformation in the Koa‘e is a pronounced east-west structure gradient.
409 In the Krafla fissure swarm, monoclines are comparatively rare and associated with smaller
410 displacement faults. They do not demonstrate a preferred spatial distribution. Surface-breaking
411 normal faults on the other hand, are found up to 20 km away from the central volcano.
412

4.2. Controls on the surface expression of extensional structures

4.2.1. Syntectonic volcanism

Most numerical and scaled-analogue models of fault growth in cohesive sequences involve uniform, constant-rate displacement boundary conditions (e.g. Grant and Kattenhorn, 2004; Holland et al., 2006, 2011; Martel and Langley, 2006). Driving stresses, and hence, strain rates in both the Koa‘e and Krafla rift settings, however, are neither uniformly distributed, nor constant through time. Extension in both areas is associated with repeated dyke injection events, the scale and timing of which are variable in time, space, and magnitude (e.g. Tryggvason, 1984; Dvorak and Dzurisin, 1993; Bjornsson et al., 2007; Delaney et al., 1998; Buck et al., 2006). Variable rates and duration of magma emplacement within the rift zones has the effect of altering local stress distributions, which in turn drives variations in strain rate and results in local strain rate gradients. This should be expected to influence segmentation patterns and fault architecture. The distribution of surface deformation styles in the Koa‘e fault system may be a record of this.

FIGURE 12 HERE

Periods of inflation and deflation within Kīlauea ’s south flank have been linked with regions of elevated concomitant seismicity below the summit and upper ERZ (Figure 12) at ~2-5 km depth (e.g. Delaney et al., 1998; Hansen et al., 2004; Baker and Amelung, 2012, Lin and Okubo, 2016). Earthquake swarms originating in the upper ERZ have been recorded to migrate into the Koa‘e fault system during intrusion events (Delaney et al., 1998), and in some instances linked to episodes of slip on major faults in the areas. The proximal distribution of surface-breaking faults in the eastern Koa‘e fault system are therefore likely to be linked to these areas of elevated

436 seismicity and magma emplacement. For instance, records of GPS data, InSAR, and field
437 observations, have revealed evidence for minor slip on the Kulanaokuaiki Fault during the
438 September 1999 dyke intrusion event (Cervelli et al., 2002) (Figure 12). This is consistent with
439 elastic dislocation models of the south flank that predict regions of high tensile stress
440 concentrations that centre on the intruded region and extend into the eastern Koa‘e (Owen et al
441 2000; Cervelli et al., 2002). The scale and distribution of such stress concentrations become a
442 function of the magnitude and location of the emplacement event, and hence, the resulting strain
443 rate along the rift zone will vary accordingly. Magmatic and seismic activity in Kīlauea ’s SWRZ,
444 by comparison, is significantly less (e.g. Dvorak and Dzurisin, 1993; Wauthier et al., 2016). During
445 the period 2005-2007 inflation episode, for example, seismicity records indicate up to ~10 events
446 per day in the SWRZ, compared to ~30 per day in the ERZ (Wauthier et al., 2016). Models of
447 magma partitioning suggest that during the period 1840-1989, ~57% of magma supplied to the
448 volcano was emplaced and erupted within the ERZ (1575 x 10^6 m^3) with only ~2% (45 x 10^6 m^3)
449 being erupted in the SWRZ (Dzurisin et al., 1984; Dvorak and Dzurisin, 1993). The result of this
450 partitioning has led to more than 20 eruptions in the ERZ since 1950, associated with deflation of
451 Kīlauea’s summit reservoir, and only two events taking place in the SWRZ. Partitioning of
452 extensional strain across the Koa‘e fault system implies that total strains are comparable across the
453 system, but spatially variable strain rates control whether faults are able to propagate straight to
454 the surface (eastern Koa‘e), or remain segmented at depth for protracted periods with slip
455 accommodated aseismically, generating surface monoclines (western Koa‘e). This is consistent
456 with volcano-tectonic seismicity modelling from Kīlauea (e.g. Wauthier et al., 2016), and other
457 volcanic faults (Toda et al., 2002; Roman and Gardine, 2013), which suggest that low rates of
458 magma emplacement produce correspondingly low strain rates that are unable to drive significant

459 seismicity. With renewed magmatic partitioning into the SWRZ during future episodes, faults in
460 western portions of the Koa‘e may therefore breach the surface and monoclines will be preserved
461 in their hanging walls.

462 In contrast, the relatively minor abundance of monoclines and dominance of larger (>10 m
463 throw) surface-breaking faults in the Krafla fissure swarm, up to 20 km away from the summit
464 does not imply the presence of a spatial strain rate gradient, indicating magma supply here and
465 related stresses are relatively uniform. Following re-surfacing, therefore, stresses and strain rates
466 are high enough for fault segments to propagate straight to the surface without folding it first. The
467 occurrence, however, of breached monoclines, though uncommon, suggests a temporal strain rate
468 gradient can also exist. In evolving volcanic rift systems, therefore, the final geometry of first-
469 order faults becomes a strain rate-dependent function of the magmatic processes taking place. This
470 dependence becomes both a spatial problem as well as a temporal one.
471

472 **4.2.2. Mechanical stratigraphy**

473 In addition to magmatically induced segmentation patterns, host rock mechanical properties are
474 also likely to play a role in the distribution and geometry of faults in the study areas. A prominent
475 cooling joint fabric and mechanical layers, in the form of bedding and physical property variations
476 (e.g. Planke, 1994; Bubeck et al., 2017a), mean that basaltic sequences are highly anisotropic and
477 host a similarly pronounced mechanical stratigraphy as have been reported for layered clastic (e.g.
478 Ferrill et al., 2017) and crystalline-clastic sequences (Walker et al., 2013). Existing studies of
479 extensional fault geometry in mechanically layered sequences have shown that the mechanical
480 properties of a deforming volume will govern segmentation patterns, and hence, the final
481 architecture of fault zones (e.g. Peacock and Sanderson, 1991; Ferrill and Morris, 2003; Schöpfer

et al., 2006; Van Gent et al., 2010; Walker et al., 2013). At the metre-scale, anisotropy within basaltic sequences pertains to varying physical and mechanical properties within individual lava units or volcaniclastic horizons, as well as networks of pre-existing cooling joints. At the tens to hundreds of metre-scale, changes in compositional layering and fluid content within the sequence should also be expected to influence the distribution and geometry of surface structures in developing volcanic rift systems.

4.3.A modified conceptual model for near-surface fault growth in basaltic sequences

Here, we present conceptual models for near-surface fault growth, based on the natural distribution and geometry of extensional structures in the Koa'e and Krafla fault systems, as an expansion of the numerical models presented by Martel and Langley (2006) and Kaven and Martel (2007). As this model is based on surface observations only, stage I is based on theoretical models of dyke-fault relationships from volcanic settings. Depending on the distribution, magnitude, and duration of individual rifting episodes, fault zones may show variable overall geometries and associated fracture densities, as a function of spatial and temporal strain rate evolution. For this reason, stage III of this model is divided into two paths that are referred to here as: a high strain rate path and a low strain rate path.

FIGURE 13 HERE

Stage I: Initial extension may result from magma release during deflation of the central reservoir where high magma pressure will drive dykes into existing adjacent joints or discontinuities. At intermediate depths, upward (or lateral) propagation, governed by the hydrofracture criterion (e.g.

505 Gudmundsson, 2011), is impeded by the presence of mechanical barriers (e.g. Bell and Kilburn,
506 2012) or when driving pressures drop (e.g. Buck et al., 2006; Rowland et al., 2007). Dyke tip
507 stresses are relieved by the growth of normal faults, which propagate along maximum tensile strain
508 trajectories within the overlying basalt cover (e.g. Hollingsworth et al., 2013).
509
510 **Stage II**: In the region ahead of upward-propagating normal faults, at a critical distance from the
511 free surface (controlled by the magnitude of the stress intensity at the fault tip), extension fractures
512 begin to localise in linear zones along pre-existing cooling joints that are optimally oriented. These
513 zones are parallel to the structures at depth and progressively lengthen downwards and laterally
514 (Figure 13, Stage 1).
515 **Stage III (low strain rate)**: During periods, or in regions of subdued magmatism, local driving
516 stresses are too low to drive significant fault slip. Under these conditions, through-going linkage
517 of fault tiplines at depth, and surface fractures, is prevented and faults will remain segmented at
518 depth. Here, they will creep aseismically, producing monoclinal folding of the layers ahead of the
519 tipline (Figure 13, Stage 2). With renewed magmatic activity, strain rates will increase once more
520 and through-going linkage will be possible. During slip accumulation, and further upward
521 propagation, surface monoclines will steepen until they are breached along newly linked fault-
522 fracture networks (Figure 13, Stage 3).
523 **Stage III (high strain rate)**: During periods, or in regions of elevated magmatism, or in the
524 absence of resistant layers, linkage of upward propagating faults, and downward propagating
525 fractures will result in through-going, surface-breaking faults. At this stage, extension is localised
526 on a smaller number of larger structures, which dominate over new fracture growth: an exponential
527 scaling is predicted (e.g. Ackerman et al., 2001). This process could take place relatively quickly

and result in through-going faults without folding of the surface (Figure 13, Stage 4). Seismicity data and eyewitness accounts, for instance, of the Kulanaokuaiki fault during the 1965 eruption of Kilauea Volcano, record evidence of crack propagation and vertical displacement occurring over the course of hours to days following the initial eruption (Fiske and Koyanagi, 1968).

In this model, monoclines are not necessarily precursory features of normal fault growth but rather a record of segmented growth, which may develop at any time within the series, depending largely on local strain rates. Breached monoclines, on the other hand, may imply a period, or region, of lower strain rate and segmentation followed by a sudden rate increase once more and through-going fault development.

An upward propagating fault model (e.g., Martel and Langley, 2006) is strongly supported by our field observations. Extension fractures are not randomly distributed across either fault system. In both settings, fractures are parallel to the trend of the rift zone and major rift faults and folds within it. Although fractures show a spatial relationship with fold curvature in some places, outer arc stretching is not the primary driving mechanism for their formation. A coupled evolution of fractures at the free surface and faults at depth, driven by stresses ahead of a blind fault tip is consistent with existing numerical predictions (e.g. Martel and Langley, 2006).

The growth of fault populations through time in developing volcanic rift systems, however, do not follow a uniform, systematic evolution; the distribution and geometry of normal faults in the Krafla fissure swarm are not always directly evolved equivalents of faults in the Koa‘e fault system. This model may account for the apparent lack of preserved monoclines in exhumed basalt-hosted fault systems (e.g. Walker et al., 2012, 2013). Although factors including pre-existing structures and mechanical stratigraphy will influence the nucleation and initial geometry of fault

structures, changes in strain rate at any stage will alter the geometry and distribution of preserved faults.

5. Conclusions

Current models for surface-breaking in faults in volcanic sequences dominantly invoke geometric or kinematic linkage as a progressive fault zone evolution. Our findings support existing models in a simple way: surface deformation is localized by normal faults that nucleate at depth and drive tensile stress concentrations ahead of the fault tip. Coupled upward propagation of fault tips at depth, and downward growth of surface fractures produces surface-breaking normal faults with prominent horizontal openings at their base. Contrary to model predictions, however, precursory monoclines are not systematic features of growth faults in basaltic sequences. We suggest that such deviations from model-predicted structural style and distribution can be explained by local variations in strain rate through time, and spatially within the actively deforming region. Strain rates within volcanic rift systems are genetically linked to magmatism and as such, surface-breaking faults within individual, or separate rift systems, may not experience a consistent evolution. Small displacement faults, therefore, will not necessarily be representative of the early stages of more evolved systems.

ACKNOWLEDGMENTS

The authors wish to extend enormous gratitude to Don Swanson at the Hawaiian Volcano Observatory, Hawai‘i, and Mike Poland (now at Cascades Volcano Observatory, Vancouver) for help and advice during field seasons to the Koa`e fault system. We further thank Don for taking the time to provide feedback on this manuscript and for generously sharing data with us. Authors Bubeck and Walker especially wish to thank Don for an unforgettable first tour of the Koa`e fault

system. We also thank the National Park Service for granting a permit to conduct fieldwork in the Koa`e fault system. Aerial LiDAR datasets were provided by the OpenTopography Facility with support from the National Science Foundation under NSF Award Numbers 1226353 & 1225810 (not related to this study). This research did not receive any specific grant from funding agencies in the public, commercial, or not-for-profit sectors. We thank Jonathan Bull for his review and extend special thanks to Michael Kettermann for his detailed and constructive review of an earlier version of this manuscript.

FIGURES

Figure 1. Measurement of fracture geometry and kinematics: extension-mode opening across pre-existing cooling joint surfaces allows the traditional measurement of opening direction, aperture, azimuth and vertical offset (where present).

Figure 2. A. Simplified structural elements map of Kīlauea Volcano: Koa`e fault system (KFS); ERZ: East Rift Zone; SWRZ: Southwest Rift Zone; HFS: Hilina Fault System. Inset shows relative position of A, on the south coast of Hawai`i. B. Map of extensional structures in the Koa`e fault system: (1) surface-breaking normal faults (yellow lines); (2) extension fracture networks (orange lines); and (3) monoclinal folds with lengths >150 m (blue lines). Bi. Rose diagram highlights the strike direction of monoclines in the Koa`e fault system. Bii. Rose diagram highlights the strike direction of 1888 mapped fracture and faults in the Koa`e fault system. C. Lower hemisphere stereographic projections showing the average strike of fault/fractures and calculated maximum horizontal extension directions for the two dominant

orientations: i) ENE-WSW striking (ERZ-parallel) structures, accommodating NNW-SSE extension; ii) NW-SE striking (ERZ-oblique) structures accommodating NE-SW extension.

Figure 3. Scaling and location of extension fracture networks. A. At the 100's of metre-scale, fracture zones are predominantly located in the footwall of faults and along the upper limb of monoclines. Zones range from 30-50 in width and extend for >1 km. Base image: aerial World-View 2 satellite image (0.5 m resolution). Inset map indicates image locations for parts A, B and C. B. At the 10's of metre-scale fractures show stepped geometries and apertures of up to ~4 m. C. At the cm-scale, fractures also demonstrate stepping trace geometries and "hook-shaped" tip geometries in the vicinity of neighbouring fracture tips. At these scales, fractures are also observed in otherwise undeformed (i.e. not folded, non-faulted) regions of the fault system.

Figure 4. Maps of 3D surface curvature derived from aerial LiDAR datasets and examples of extension fracture distribution in the Koa`e fault system. A positive curvature (warm colours) indicates the surface is upwardly convex; a negative curvature (cold colours) indicates the surface is upwardly concave. A. Fracture networks are present in areas of the fault system where there is no topographic expression of fault slip (i.e. monoclines, or fault scarps). Anomalous regions of curvature are associated with tumuli and the general morphology of the lava field. B. Fracture networks occur along the upper limb of monoclines where they are not spatially associated with regions of maximum curvature across monoclines. C. Fracture networks show a strong spatial relationship with regions of maximum curvature across monoclines.

Figure 5. Examples of monocline type in the Koa`e fault system. Inset map indicates image locations for parts A and B. A. Laterally continuous monoclines with fold limbs that dip gently and vary from a 2 m to ~ 10 m in amplitude. Zones of fractures are found along the upper limbs and rubbly toes at the base. Crests can be traced for over 1 km. B. Laterally discontinuous monoclines form densely fractured, often disintegrated blocks in the hanging wall of faults. Lengths vary from 10 m to 150 m and amplitudes from 2 m to 15 m. Solid red line in part A highlights monocline profile. Dashed blue lines: extent of continuous monocline; dashed orange line indicates extent of discontinuous monocline; dashed red lines: continuous open fracture; dashed yellow lines: extent of hanging wall buckles.

Figure 6. A. Map view of the continuous monocline shown in Figure 5, showing the distribution of extension fractures along the upper limb (dotted red lines). For location, please refer to the inset map for Figure 5. B. Cross-sections across the monocline in part A. Transect locations are show in part A. Transects 1-3 and 6 show steep, rounded monoclines with extension fractures along the region of maximum curvature. Transects 4 and 5 show a region of the monocline that has been breached by fault segments. The extent of this breaching is spatially limited. C: A map highlighting changes in 3D surface curvature across the monocline in part A. D. A slope map across the monocline in part A. Slope angles for the monocline limb range from ~12-25˚ with these values varying along-strike. Base image in A is an aerial World-View 2 satellite image (0.5 m resolution). Terrain data in parts C and D are derived from aerial LiDAR dataset (0.5 m resolution) provided by OpenTopography and generated in ArcGIS® software by Esri.

639 **Figure 7**. Map view of monocline types. A. Continuous monocline with a network of extension
640 fractures along the upper limb. Limbs dip towards the north at ~10°. Breached continuous
641 monoclines are observed, but less commonly than unbreached. B. Fault tip monoclines between
642 en echelon segments along the Ohale Fault. Tip monoclines dip parallel to the bounding segments
643 by ~10°. C. Discontinuous monocline blocks (dotted, yellow lines), isolated between normal fault
644 segments (heavy red line), connected by collinear extension fractures (dotted red line) along the
645 upper limb to form continuous open fractures that decouple the monocline from the footwall. These
646 monoclines dip more steeply (~30°) from a central amplitude maxima, to zero at the lateral edges.
647 Breached discontinuous monoclines have not been observed. Base images: World-View 2 satellite
648 image (0.5 m resolution).
649
650 **Figure 8**. Examples of surface-breaking normal fault segments in the Koa'e fault system. Inset
651 map indicates location for images in Part A and B. A. The largest vertical offsets (up to ~15m)
652 and greatest proportion of fault scarps are found on the Kulanaokuaiki ("Shaking Spine") fault. B.
653 Where present, scarps show a significant component of horizontal opening and offset planar
654 footwall and hanging wall ground surfaces. Also present along many (but not all) faults in the
655 Koa'e fault system are hanging wall buckles that occur ahead of both fault scarps and monoclinal
656 structures. Dashed orange line: extent of discontinuous monocline; dashed blue lines: extent of
657 continuous monocline; dashed red lines: continuous open fracture; dashed yellow lines: extent of
658 hanging wall buckles.
659
660 **Figure 9.** A. Map of Iceland highlighting the major tectonic elements: Reykjanes Ridge (RR);
661 the Kolbeinsey Ridge (KR); West Volcanic Zone (WVZ); East Volcanic Zone (EVZ); Neo-

662 Volcanic Zone (NVZ: the axial rift zone); Askja volcanic centre (As); Fremri-Namur volcanic
663 centre (Fr); Krafla volcanic centre, (highlighted blue; Kr); Theistareykir volcanic centre (Th); the
664 Dalvik lineament (DF), the Husavik-Flatey Fault (HF) and the Grimsey lineament (GF). B.
665 Location of study area in the Gjastykki Valley within the Krafla fissure swarm. C. Mapped faults
666 and extension/oblique-extensional fractures in the study area. Image locations and view
667 directions in Figures 10 and 11 are indicated. Ci. Rose diagram highlights the strike of normal
668 faults and fractures in the Krafla fissure swarm. D. Lower hemisphere stereographic projections
669 showing the average strike of fault/fractures and calculated maximum horizontal extension
670 directions for the three dominant orientations: i) NNE-SSW striking faults and fractures,
671 accommodating WNW-ESE extension; ii) WNW-ESE striking fractures, accommodating NNE-
672 SSW extension; iii) NW-SE striking faults and fractures, accommodating ENE-WSW extension.
673
674 **Figure 10.** Examples of surface-breaking normal fault segments in the Gjastykki area of the Krafla
675 fissure swarm. A. Subvertical normal faults with throws of up to 25-30 m and offset planar footwall
676 and hanging wall surfaces. B. Rift faults show prominent horizontal openings of 2-4 m and
677 overlapping geometries with obliquely-oriented linking segments.
678
679 **Figure 11.** Examples of monoclines in the Krafla fissure swarm. A. Monoclines show amplitudes
680 of up to ~3 m with open fractures along their upper limbs that are co-linear with fault segments on
681 either side. B. Breached monocline observed in the hangingwall of a surface-breaking normal fault
682 with vertical offset of up 2-3 m. Along the fault in the image, an additional monocline has
683 developed further into the hanging wall. C. Monoclines can also be strongly fragmented and show
684 steep rotations. In all examples, their lateral extent is <50 m.

Figure 12. Distribution of surface-breaking normal faults and monoclinal folds across the Koa`e fault system. Blue circles represent focal mechanisms in the summit, upper ERZ, and upper SWRZ regions of Kīlauea Volcano from the period 1986-2009. Contours highlight the density of events based on approx. 3000 focal mechanisms recorded in this region. Earthquake data reproduced from Lin and Okubo, 2016. ~90% of focal mechanisms in the catalog are small earthquakes (96% <M2.5), from shallow depths (i.e. <13 km); half of the focal mechanisms are recorded from 2-5 km depth. Dyke intrusion events taken from Baker and Amelung, 2015 and Cervelli et al., 2002.

Figure 13. Conceptual model for growth faults in volcanic rift zones with spatially (and temporally) variable strain rates, with field examples of the model stages 1-4 from the Koa`e and Krafla fault systems. Principal stress axes (red arrows) represent the regional stress state acting on the rift zone. 1. Precursory extension fractures localize in narrow zones at the free surface ahead of blind normal faults. 2. In regions of the rift zone where strain rates are high, normal faults propagate rapidly upwards through the sequence and link with downward propagating surface fractures, producing fault scarps. A lack of preserved monocline indicates strain rates have remained high since the last resurfacing event. Antithetic faults may develop from points of stress concentration, causing a rotation of the hanging wall block above them. 3. In regions of the rift zone where strain rates are low, faults remain at depth where they accumulate slip asesimically and gradually deform the free surface ahead of the tipline into monoclines. 4. In regions of the rift zone that experience episodically high strain rates, faults may spend protracted periods segmented at depth, followed by a rapid propagation phase that results in linkage with surface fractures and breaching of earlier formed monoclines at the free surface.

708

709 **REFERENCES CITED**

710 Ackermann, R. V., Schlische, R. W. & Withjack, M. O. 2001. The geometric and statistical
711 evolution of normal fault systems: an experimental study of the effects of mechanical layer
712 thickness on scaling laws. *Journal of Structural Geology,* 23**,** 1803-1819.

713 Acocella, V., Gudmundsson, A. & Funicello, R. 2000. Interaction and linkage of extension
714 fractures and normal faults: examples from the rift zone of Iceland. *Journal of Structural*
715 *Geology*, 22, 1233-1246.

716 Anderson, S. R. & Bowers, B. 1995. Stratigraphy of the unsaturated zone and uppermost part of
717 the Snake River Plain aquifer at Test Area North, Idaho National Engineering Laboratory,
718 Idaho. *Water Resources Investigations Report 95-4130. US Geological Survey*.

719 Baker, S. & Amelung, F. 2012. Top-down inflation and deflation at the summit of Kīlauea
720 Volcano, Hawai‘i observed with InSAR. *Journal of Geophysical Research: Solid Earth,* 117**,**
721 n/a-n/a.

722 Bell, A. F. & Kilburn, C. R. J. 2012. Precursors to dyke-fed eruptions at basaltic volcanoes:
723 insights from patterns of volcano-tectonic seismicity at Kilauea volcano, Hawaii. *Bulletin of*
724 *Volcanology,* 74**,** 325-339.

725 Bjornsson, A., Johnsen, G., Sigurdsson, S., Thorbergsson, G. & Tryggvason, E. 1978. Rifting of
726 the plate boundary in North Iceland 1975-1978. National Energy Authority Report 0S-JHD-78-
727 21. Nordic Volcanological Institute: University of Iceland.

728 Bjornsson, A., Saemundsson, K., Sigmundsson, F., Halldorsson, P., Sigbjornsson, R. &
729 Snaebjornsson, J. T. 2007. Geothermal projects in NE Iceland at Krafla, Bjarnarflag, Gjastykki
730 and Theistareykir: assessment of geo-hazards affecting energy production and transmission

systems emphasizing structural design criteria and mitigation of risk. Landsvirkjun report LV-2007/075.

Brandsdottir, B. & Einarsson, P. 1979. Seismic activity associated with the September 1977 deflation of the Krafla central volcano in north-eastern Iceland. *Journal of Volcanology and Geothermal Research*, 6, 197-212.

Bubeck, A., Walker, R. J., Healy, D., Dobbs, M. & Holwell, D. A. 2017a. Pore geometry as a control on rock strength. *Earth and Planetary Science Letters,* 457**,** 38-48.

Bubeck, A., Walker, R. J., Imber, J., Holdsworth, R. E., MacLeod, C. J., & Holwell, D. A. 2017b. Extension parallel to the rift zone during segmented fault growth: application to the evolution of the NE Atlantic. *Solid Earth*, *8*(6), 1161.

Buck, W. R., Einarsson, P. & Brandsdóttir, B. 2006. Tectonic stress and magma chamber size as controls on dike propagation: Constraints from the 1975–1984 Krafla rifting episode. *Journal of Geophysical Research*, 111, 1-15.

Caprarelli, G., Pondrelli, M., Di Lorenzo, S., Marinangeli, L., Ori, G. G., Greeley, R., & Neukum, G. (2007). A description of surface features in north Tyrrhena Terra, Mars: Evidence for extension and lava flooding. *Icarus*, *191*(2), 524-544.

Casey, M., Ebinger, C., Keir, D., Gloaguen, R. & Mohamed, F. (eds.) 2006. *Strain accommodation in transitional rifts: extension by magma intrusion and faulting in Ethiopian rift magmatic segments,* The Geological Society of London: Geological Society, London, Special Publications.

Cervelli, P., Segall, P., Amelung, F., Garbeil, H., Meertens, C., Owen, S., Miklius, A. & Lisowski, M. 2002. The 12 September 1999 Upper East Rift Zone dike intrusion at Kilauea Volcano, Hawaii. *Journal of Geophysical Research: Solid Earth,* 107**,** ECV 3-1-ECV 3-13.

754 Crider, J. G. & Pollard, D. D. 1998. Fault linkage: Three-dimensional mechanical interaction
755 between echelon normal faults. *Journal of Geophysical Research*, 103, 24,373-24,391.
756 Dauteuil, O., Angelier, J., Bergerat, F., Verrier, S. & Villemin, T. 2001. Deformation partitioning
757 inside a fissure swarm of the northern icelandic rift. *Journal of Structural Geology,* 23**,** 1359-
758 1372.
759 Davison, I., Stasiuk, S., Nuttall, P. & Keane, P. 2004. Sub-basalt hydrocarbon prospectivity in the
760 Rockall, Faroe-Shetland an Møre Basins, NE Atlantic. Geological Society London. In: Vining,
761 B.A. and Pickering, S.C. (eds.) Petroleum Geology: from mature basins to new frontiers.
762 *Proceedings of the 7th Petroleum Geology Conference,* 1025-1032. Petroleum Geology
763 Conferences Ltd, published by the Geological Society, London.
764 Delaney, P. T., Denlinger, R. P., Lisowski, M., Miklius, A., Okubo, P. G., Okamura, A. T. & Sako,
765 M. K. 1998. Volcanic Spreading at Kilauea, 1976–1996. *Journal of Geophysical Research*, 103,
766 18,003-18,023.
767 Delaney, P. T., Fiske, R. S., Miklius, A., Okamura, A. T. & Sako, M. K. 1990. Deep magma
768 body beneath the summit and rift zones of Kilauea Volcano, Hawaii. *Science* 247.4948
769 (1990): 1311-1316.
770 Denlinger, R. P. & Okubo, P. G. 1995. Structure of the mobile south flank of Kilauea Volcano,
771 Hawaii. *Journal of Geophysical Research,* 100**,** 24499.
772 Duffield, W. A. 1975. Structure and Origin of the Koae Fault System, Kilauea Volcano, Hawaii.
773 *Geological Survey Professional Paper 856.*
774 Duffield, W. A., Christiansen, R. L., Koyanagi, R. Y. & Peterson, D. W. 1982a. Storage, migration
775 and eruption of magma at Kilauea Volcano, Hawaii, 1971-1972. *Journal of Volcanology and*
776 *Geothermal Research*, 13, 273-307.

Dvorak, J. J. & Dzurisin, D. 1993. Variations in Magma Supply Rate at Kilauea Volcano, Hawaii. *Journal of Geophysical Research-Solid Earth*, 98, 22255-22268.

Dzurisin, D., Koyanagi, R. Y. & English, T. T. 1984. Magma supply and storage at Kiluea Volcano, Hawaii, 1956-1983. *Journal of Volcanology and Geothermal Research*, 21, 177-206.

Escartín, J., Leclerc, F., Olive, J. A., Mevel, C., Cannat, M., Petersen, S., Augustin, N., Feuillet, N., Deplus, C., Bezos, A., Bonnemains, D., Chavagnac, V., Choi, Y., Godard, M., Haaga, K. A., Hamelin, C., Ildefonse, B., Jamieson, J. W., John, B. E., Leleu, T., Macleod, C. J., Massot-Campos, M., Nomikou, P., Paquet, M., Rommevaux-Jestin, C., Rothenbeck, M., Steinführer, A., Tominaga, M., Triebe, L., Campos, R., Gracias, N., Garcia, R., Andreani, M. & Vilaseca, G. 2016. First direct observation of coseismic slip and seafloor rupture along a submarine normal fault and implications for fault slip history. *Earth and Planetary Science Letters,* 450**,** 96-107.

Faulds, J. E. & Varga, R. J. 1998. The role of accommodation zones and transfer zones in the regional segmentation of extended terranes. In: Faulds, J. E and Stewart, J. H. (eds.) Accommodation Zones and Transfer Zones: the Regional Segmentation of the Basin and Range Province: Boulder, Colorado. *Geological Society of America Special Paper* 323, 1-45.

Ferrill, D. A. & Morris, A. P. 2001. Displacement gradient and deformation in normal fault systems. *Journal of Structural Geology*, 23, 619-638.

Ferrill, D. A. & Morris, A. P. 2003. Dilational normal faults. *Journal of Structural Geology,* 25**,** 183-196.

Ferrill, D. A., Morris, A. P., Mcginnis, R. N., Smart, K. J., Wigginton, S. S. & Hill, N. J. 2017. Mechanical stratigraphy and normal faulting. *Journal of Structural Geology,* 94**,** 275-302.

799 Fiske R.S., Koyanagi R.Y. 1968. The December 1965 Eruption of Kilauea Volcano, Hawaii.
800 Geological Survey Professional Paper. No. 607, 1-21.
801 Forslund, T. & Gudmundsson, A. 1991. Crustal spreading due to dikes and faults in southwest
802 Iceland. *Journal of Structural Geology*, 13, 443-457.
803 Grant, J. V. & Kattenhorn, S. A. 2004. Evolution of vertical faults at an extensional plate
804 boundary, southwest Iceland. *Journal of Structural Geology*, 26, 537-557.
805 Gudmundsson, A. 2011. *Rock Fractures in Geological Processes,* Cambridge, UK, Cambridge
806 University Press.
807 Hansen, S., Thurber, M., Mandernach, F., Haslinger, F. & Doran, C. 2004. Seismic velocity and
808 attenuation structure of the East Rift Zone and south flank of Kilauea Volcano, Hawaii.
809 *Bulletin of the seismological society of america,* 94.
810 Hauber, E., Grott, M., & Kronberg, P. (2010). Martian rifts: Structural geology and
811 geophysics. *Earth and Planetary Science Letters*, *294*(3-4), 393-410.
812 Helm-Clark, C. M., Rodgers, D. W. & Smith, R. P. 2004. Borehole geophysical techniques to
813 define stratigraphy, alteration and aquifers in basalt. *Journal of Applied Geophysics*, 55, 3-38.
814 Hjartardóttir, Á. R., Einarsson, P., Bramham, E. & Wright, T. J. 2012. The Krafla fissure swarm,
815 Iceland, and its formation by rifting events. *Bulletin of Volcanology*, 74, 2139-2153.
816 Holland, M., Urai, J. L. & Martel, S. J. 2006. The internal structure of fault zones in basaltic
817 sequences. *Earth and Planetary Science Letters*, 248, 301-315.
818 Hollingsworth, J., Leprince, S., Ayoub, F. & Avouac, J. P. 2013. New constraints on dike
819 injection and fault slip during the 1975-1984 Krafla rift crisis, NE Iceland. *Journal of*
820 *Geophysical Research: Solid Earth,* 118**,** 3707-3727.

821 Hus, R., De Batist, M., Klerkx, J. & Matton, C. 2006. Fault linkage in continental rifts: structure
822 and evolution of a large relay ramp in Zavarotny; Lake Baikal (Russia). *Journal of Structural*
823 *Geology*, 28, 1338-1351.
824 Kaven, J. O. & Martel, S. J. 2007. Growth of surface-breaching normal faults as a three-
825 dimensional fracturing process. *Journal of Structural Geology*, 29, 1463-1476.
826 Klein, F. W., Koyanagi, R. Y., Nakata, J. S. & Tanigawa, W. R. 1987. Volcanism in Hawaii. In:
827 Decker, R. W., Wright, T. L. and Stuaffer, P. H. (eds.) US Geological Survey Professional
828 Paper 1350.
829 Lambiase, J. J. & Bosworth, W. 1995. Structural controls on sedimentation in continental rifts.
830 In: LAMBIASE, J. J. (ed.) Hydrocarbon habitat in rift basins. Geological Society Special
831 Publication no. 80. The Geological Society, London.
832 Le Corvec, N. & Walter, T. R. 2009. Volcano spreading and fault interaction influenced by rift
833 zone intrusions: Insights from analogue experiments analyzed with digital image correlation
834 technique. *Journal of Volcanology and Geothermal Research,* 183**,** 170-182.
835 Lin, G. & Okubo, P. G. 2016. A large refined catalog of earthquake relocations and focal
836 mechanisms for the Island of Hawai‘i and its seismotectonic implications. *Journal of*
837 *Geophysical Research: Solid Earth*.
838 Lin, G., Amelung, F., Lavallee, Y. & Okubo, P. G. 2014. Seismic evidence for a crustal magma
839 reservoir beneath the upper east rift zone of Kilauea volcano, Hawaii. *Geology,* 42**,** 187-190.
840 Long, J. J. & Imber, J. 2010. Geometrically coherent continuous deformation in the volume
841 surrounding a seismically imaged normal fault-array. *Journal of Structural Geology*, 32, 222-
842 234.

843 Maerten, L., Gillespie, P. & Pollard, D. D. 2002. Effects of local stress perturbation on secondary
844 fault development. *Journal of Structural Geology*, 24, 145-153.
845 Manzocchi, T., Childs, C. & Walsh, J. J. 2010. Faults and fault properties in hydrocarbon flow
846 models. *Geofluids*, No. 10, 94-113.
847 Martel, S. J. & Langley, J. S. 2006. Propagation of normal faults to the surface in basalt, Koa'e
848 fault system, Hawaii. *Journal of Structural Geology*, 28, 2123-2143.
849 Michie, E. a. H., Haines, T. J., Healy, D., Neilson, J. E., Timms, N. E. & Wibberley, C. a. J.
850 2014. Influence of carbonate facies on fault zone architecture. *Journal of Structural Geology,*
851 65**,** 82-99.
852 Morley, C. K., Nelson, R. A., Patton, T. I. & Munn, S. G. 1990. Transfer zones in the East Africa
853 Rift System and their relevance to hydrocarbon exploration in rifts. *The American Association*
854 *of Petroleum Geologists Bulletin*, 74, 1234-1253.
855 Nahm, A. L., & Kattenhorn, S. A. 2015. A unified nomenclature for tectonic structures on the
856 surface of Enceladus. *Icarus*, *258*, 67-81.
857 Nahm, A. L. & Schultz, R. A. 2015. Rupes Recta and the geological history of the Mare Nubium
858 region of the Moon: insights from forward mechanical modelling of the 'Straight Wall'.
859 *Geological Society, London, Special Publications,* 401**,** 377-394.
860 Neal, C. A. & Lockwood, J. P. 2003. Geologic map of the summit region of Kilauea volcano,
861 Hawaii. *USGS Geologic Investigation Series,* I-2759.
862 Nixon, C. W., Sanderson, D. J., Dee, S. J., Bull, J. M., Humphreys, R. J. & Swanson, M. H.
863 2014. Fault interactions and reactivation within a normal-fault network at Milne Point,
864 Alaska. *The American Association of Petroleum Geologists Bulletin*, 98, 2081-2107.

865 Opheim, J. A. & Gudmundsson, A. 1989. Formation and geometry of fractures, and related
866 volcanism, of the Krafla fissure swarm, northeast Iceland. *Geological Society of America*
867 *Bulletin,* 101**,** 1608-1622.
868 Owen, S., Segall, P., Lisowski, M., Miklius, A., Denlinger, R. P. & Sako, M. 2000. Rapid
869 deformation of Kilauea Volcano: Global Positioning System measurements between 1990 and
870 1996. *Journal of Geophysical Research,* 105**,** 18983.
871 Peacock, D. C. P. & Parfitt, E. A. 2002. Active relay ramps and normal fault propagation on
872 Kilauea Volcano, Hawaii. *Journal of Structural Geology*, 24, 729-742.
873 Peacock, D. C. P. & Sanderson, D. J. 1991. Displacements, segment linkage and relay ramps in
874 normal fault zones. *Journal of Structural Geology*, 13, 721-733.
875 Peacock, D. C. P. 2002. Propagation, interaction and linkage in normal fault systems. *Earth*
876 *Science Reviews*, 58, 121-142.
877 Planke, S., Alvestad, E. & Eldhom, O. 1999. Seismic characteristics of basaltic extrusive and
878 intrusive rocks. *The Leading Edge***,** 342-348.
879 Plattner, C., Amelung, F., Baker, S., Govers, R. & Poland, M. 2013. The role of viscous magma
880 mush spreading in volcanic flank motion at Kīlauea Volcano, Hawai‘i. *Journal of Geophysical*
881 *Research: Solid Earth,* 118**,** 2474-2487.
882 Podolsky, D. M. W. & Roberts, G. P. 2008. Growth of the volcano-flank Koa’e fault system,
883 Hawaii. *Journal of Structural Geology,* 30**,** 1254-1263.
884 Poland, M. P., Miklius, A., Sutton, A. J. & Thornber, C. R. 2012. A mantle-driven surge in magma
885 supply to Kilauea Volcano during 2003-2007. *Nature Geoscience*, 5, 295-300.
886 Poland, M.P., Miklius, A., and Montgomery-Brown, E.K., 2014, Magma supply, storage, and
887 transport at shield-stage Hawai‘ian volcanoes, *in* Poland, M.P., Takahashi, T.J., and

Landowski, C.M., eds., Characteristics of Hawai‘ian volcanoes: U.S. Geological Survey Professional Paper 1801, p. 179–234.

Roman, D. C. & Gardine, M. D. 2013. Seismological evidence for long-term and rapidly accelerating magma pressurization preceding the 2009 eruption of Redoubt Volcano, Alaska. *Earth and Planetary Science Letters,* 371-372**,** 226-234.

Rowland, J. V., Baker, E., Ebinger, C. J., Keir, D., Kidane, T., Biggs, J., Hayward, N. & Wright, T. J. 2007. Fault growth at a nascent slow-spreading ridge: 2005 Dabbahu rifting episode, Afar. *Geophysical Journal International,* 171**,** 1226-1246.

Rubin, A. M. 1992. Dike-induced faulting and graben subsidence in volcanic rift zones. *Journal of Geophysical Research: Solid Earth*, 97, 1839-1858.

Sæmundsson, K. 1974. Evolution of the axial rifting zone in northern Iceland and the Tjörnes Fracture Zone. *Geological Society of America Bulletin*, 85, 495-504.

Schöpfer, M. P. J., Childs, C. & Walsh, J. J. 2006. Localisation of normal faults in multilayer sequences. *Journal of Structural Geology*, 28, 816-833.

Schultz, R. A., Hauber, E., Kattenhorn, S. A., Okubo, C. H., & Watters, T. R. 2010. Interpretation and analysis of planetary structures. *Journal of Structural Geology*, *32*(6), 855-875.

Seebeck, H., Nicol, A., Walsh, J. J., Childs, C., Beetham, R. D. & Pettinga, J. 2014. Fluid flow in fault zones from an active rift. *Journal of Structural Geology*, 62, 52-64.

Segall, P. & Pollard, D. D. 1980. Mechanics of discontinuous faults. *Journal of Geophysical Research*, 85, 4337-4350.

909 Sharp, I., Gawthorpe, R. L., Armstrong, B. & Underhill, J. R. 2000. Propagation history and
910 passive rotation of mesoscale normal faults: implications for syn-rift stratigraphic
911 development. *Basin Research*, 12, 285-305.
912 Soule, S. A., Escartín, J. & Fornari, D. J. 2009. A record of eruption and intrusion at a fast
913 spreading ridge axis: Axial summit trough of the East Pacific Rise at 9-10°N. *Geochemistry,*
914 *Geophysics, Geosystems,* 10.
915 Swanson, D. A., Duffield, W. A. & Fiske, R. S. 1976. Displacement of the south flank of Kilauea
916 Volcano: the result of forceful intrusion of magma into the rift zones. *US Geological Survey*
917 *Professional Paper*, 963.
918 Tanaka, K., Rodriguez, J., Skinnerjr, J., Bourke, M., Fortezzo, C., Herkenhoff, K., Kolb, E. &
919 Okubo, C. 2008. North polar region of Mars: Advances in stratigraphy, structure, and
920 erosional modification. *Icarus,* 196**,** 318-358.
921 Tentler, T. & Acocella, V. 2010. How does the initial configuration of oceanic ridge segments
922 affect their interaction? Insights from analogue models. *Journal of Geophysical Research*, 115,
923 1-16.
924 Toda, S., Stein, R. S. & Sagiya, T. 2002. Evidence from AD 2000 Izu islands earthquake swarm
925 that stressing rate governs seismicity. *Nature,* 419.
926 Tryggvason, E. 1984. Widening of the Krafla fissure swarm during the 1975-1981 volcano-
927 tectonic episode. *Bulletin of Volcanology*, 47-1, 47-69.
928 Tryggvason, E. 1986. Multiple magma reservoirs in a rift-zone volcano - ground deformation and
929 magma transport during the September 1984 eruption of Krafla, Iceland. *Journal of*
930 *Volcanology and Geothermal Research*, 28, 1-44.

931 Van Gent, H. W., Holland, M., Urai, J. L., & Loosveld, R. (2010). Evolution of fault zones in
932 carbonates with mechanical stratigraphy–Insights from scale models using layered cohesive
933 powder. *Journal of Structural Geology*, *32*(9), 1375-1391.
934 Vaz, D. A., Spagnuolo, M. G., & Silvestro, S. (2014). Morphometric and geometric
935 characterization of normal faults on Mars. *Earth and Planetary Science Letters*, *401*, 83-94.
936 Villemin, T. & Bergerat, F. 2013. From surface fault traces to a fault growth model: The Vogar
937 Fissure Swarm of the Reykjanes Peninsula, Southwest Iceland. *Journal of Structural Geology,*
938 51**,** 38-51.
939 Walker, R. J., Holdsworth, R. E., Imber, J. & Ellis, D. 2012. Fault-zone evolution in layered
940 basalt sequences: A case study from the Faroe Islands, NE Atlantic margin. *Geological*
941 *Society of America Bulletin*, 124, 1382-1393.
942 Walker, R. J., Holdsworth, R. E., Imber, J., Faulkner, D. R. & Armitage, P. J. 2013. Fault zone
943 architecture and fluid flow in interlayered basaltic volcaniclastic-crystalline sequences.
944 *Journal of Structural Geology*, 51, 92-104.
945 Walsh, J. J., Bailey, W. R., Childs, C., Nicol, A. & Bonson, C. G. 2003. Formation of segmented
946 normal faults: a 3D perspective. *Journal of Structural Geology*, 25, 1251-1262.
947 Wauthier, C., Roman, D. C. & Poland, M. P. 2016. Joint analysis of geodetic and earthquake
948 fault-plane solution data to constrain magmatic sources: A case study from Kīlauea Volcano.
949 *Earth and Planetary Science Letters,* 455**,** 38-48.
950 Wright, T. J., Sigmundsson, F., Pagli, C., Belachew, M., Hamling, I. J., Brandsdottir, B., Keir, A.,
951 Pedersen, R., Ayele, A., Ebinger, C., Einarsson, P., Lewi, E. & Calais, E. 2012. Geophysical
952 constraints on the dynamics of spreading centres from rifting episodes on lands. *Nature*
953 *Geoscience*, 5, 242-250.

954 Wright, T. L. & Klein, F. W. 2006. Deep magma transport at Kilauea volcano, Hawaii. *Lithos,* 87**,**
955 50-79.
956

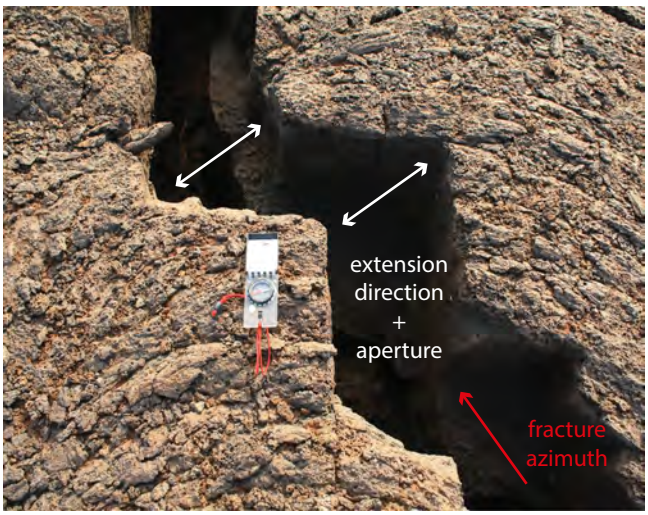

Figure 1. Measurement of fracture geometry and kinematics: extension-mode opening across pre-existing cooling joint surfaces allows the traditional measurement of opening direction, aperture, azimuth and vertical offset (where present).

Figure 2
W: 121 mm
H: 191.5 mm
(double column width)

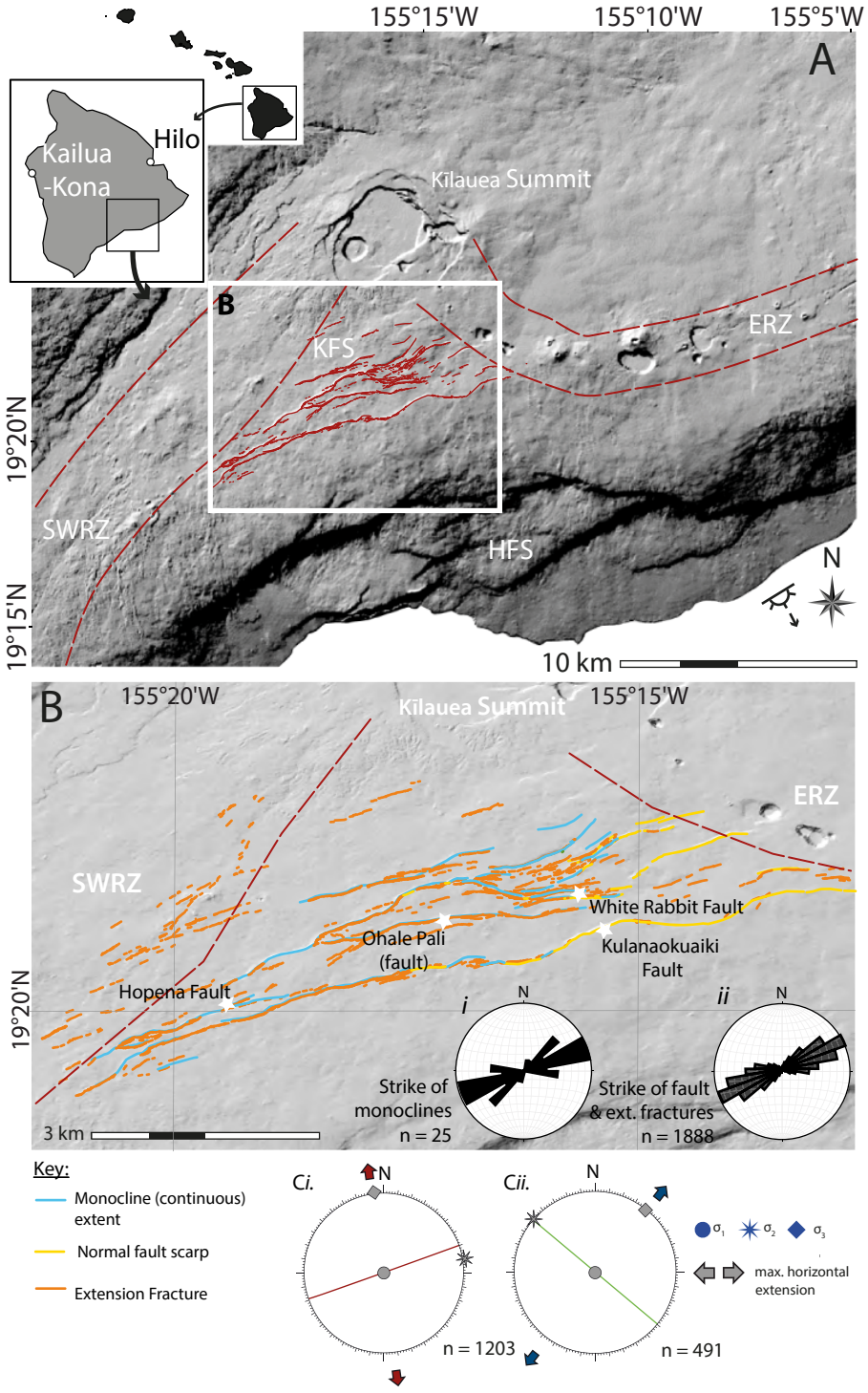

Figure 2. A. Simplified structural elements map of Kīlauea Volcano: Koa`e fault system (KFS); ERZ: East Rift Zone; SWRZ: Southwest Rift Zone; HFS: Hilina Fault System. Inset shows relative position of A, on the south coast of Hawai`i. B. Map of extensional structures in the Koa`e fault system: (1) surface-breaking normal faults (yellow lines); (2) extension fracture networks (orange lines); and (3) monoclinal folds with lengths >150 m (blue lines). B*i*. Rose diagram highlights the strike direction of monoclines in the Koa`e fault system. B*ii*. Rose diagram highlights the strike direction of 1888 mapped fracture and faults in the Koa`e fault system. C. Lower hemisphere stereographic projections showing the average strike of fault/fractures and calculated maximum horizontal extension directions for the two dominant orientations: i) ENE-WSW striking (ERZ-parallel) structures, accommodating NNW-SSE extension; ii) NW-SE striking (ERZ-oblique) structures accommodating NE-SW extension.

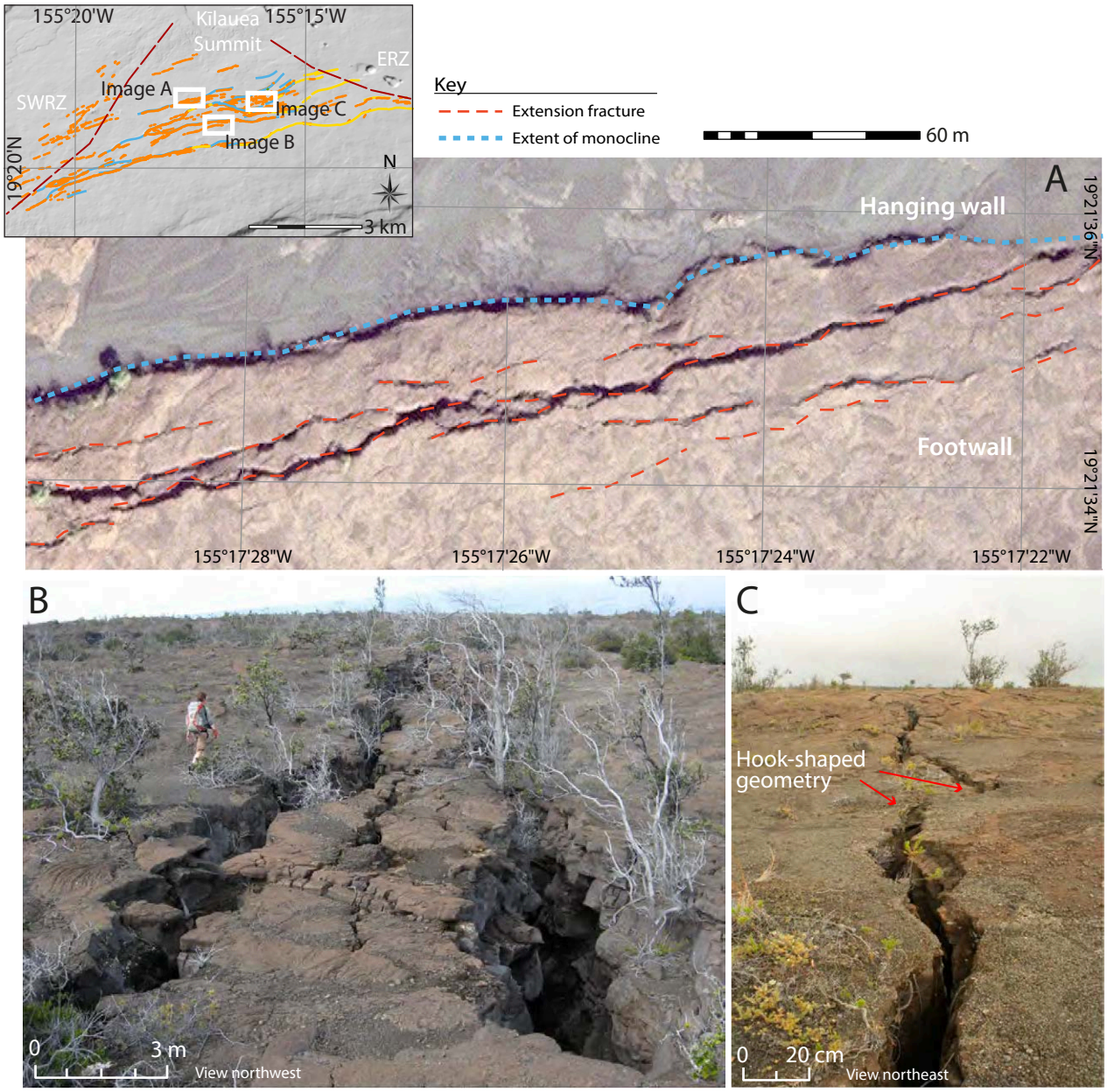

Figure 3. Scaling and location of extension fracture networks. A. At the 100's of metre-scale, fracture zones are predominantly located in the footwall of faults and along the upper limb of monoclines. Zones range from 30-50 in width and extend for >1 km. Base image: aerial World-View 2 satellite image (0.5 m resolution). Inset map indicates image locations for parts A, B and C. B. At the 10's of metre-scale fractures show stepped geometries and apertures of up to ~4 m. C. At the cm-scale, fractures also demonstrate stepping trace geometries and "hook-shaped" tip geometries in the vicinity of neighbouring fracture tips. At these scales, fractures are also observed in otherwise undeformed (i.e. not folded, non-faulted) regions of the fault system.

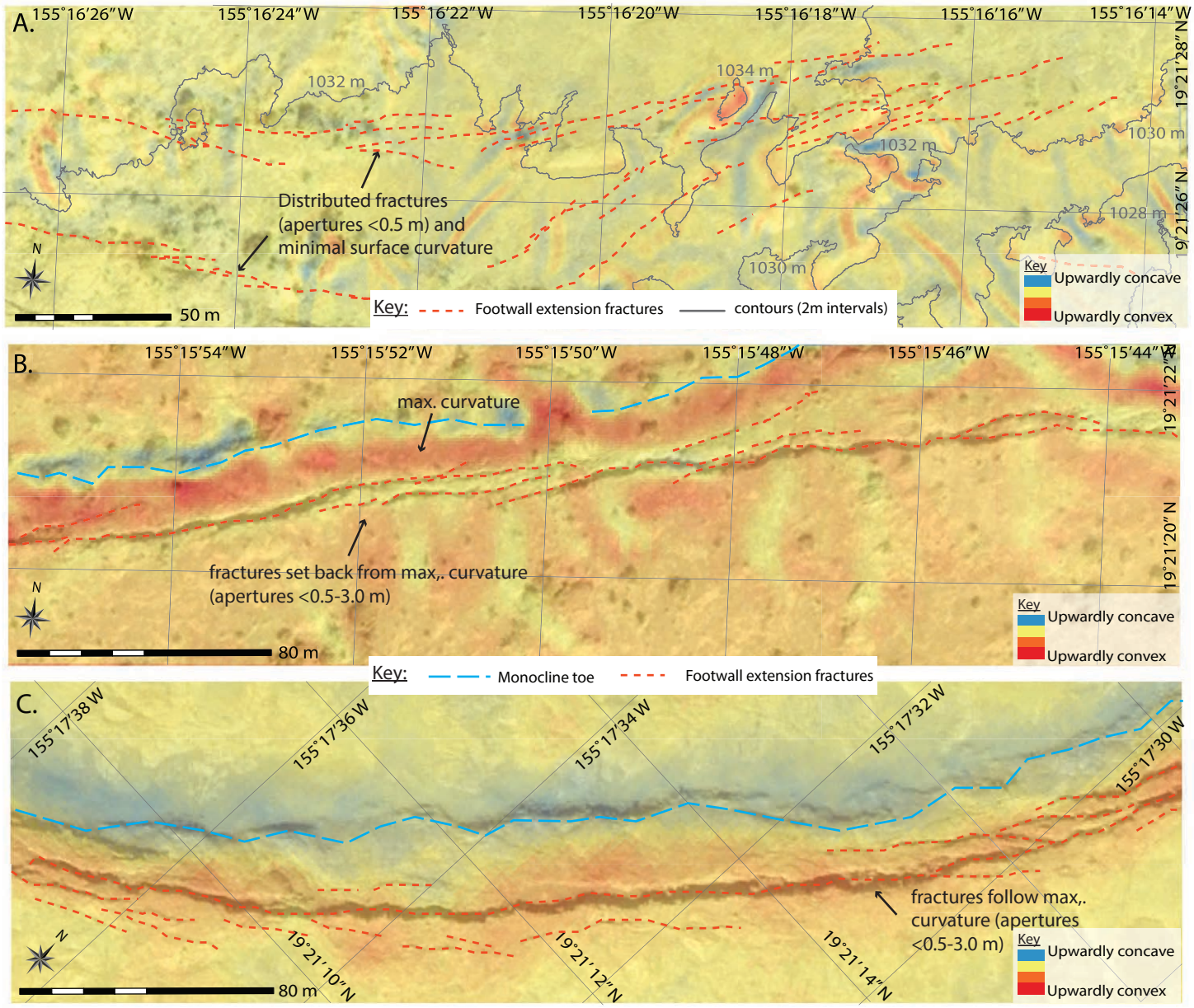

Figure 4. Maps of 3D surface curvature derived from aerial LiDAR datasets and examples of extension fracture distribution in the Koa`e fault system. A positive curvature (warm colours) indicates the surface is upwardly convex; a negative curvature (cold colours) indicates the surface is upwardly concave. A. Fracture networks are present in areas of the fault system where there is no topographic expression of fault slip (i.e. monoclines, or fault scarps). Anomalous regions of curvature are associated with tumuli and the general morphology of the lava field. B. Fracture networks occur along the upper limb of monoclines where they are not spatially associated with regions of maximum curvature across monoclines. C. Fracture networks show a strong spatial relationship with regions of maximum curvature across monoclines.

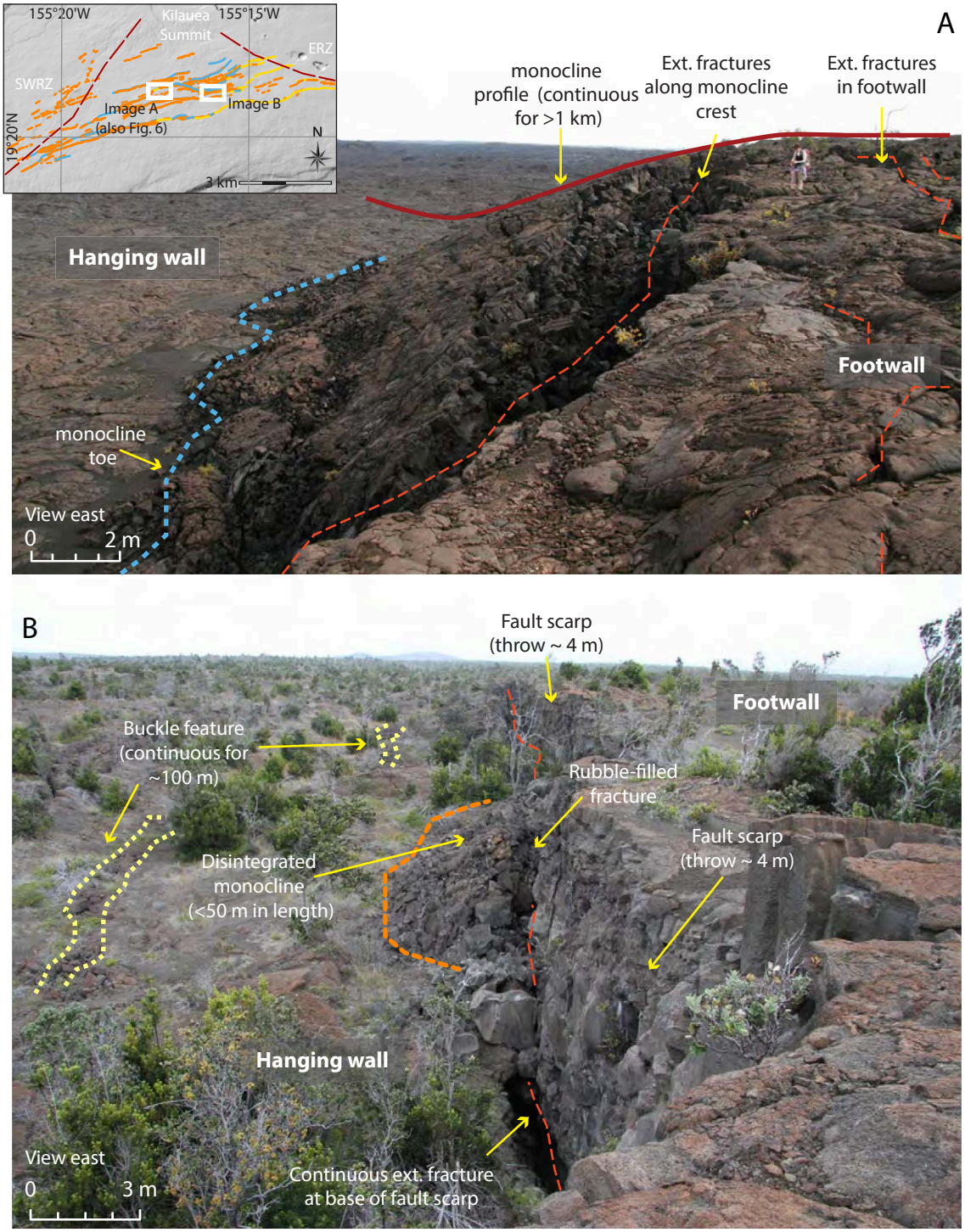

Figure 5. Examples of monocline type in the Koa`e fault system. Inset map indicates image locations for parts A and B. A. Laterally continuous monoclines with fold limbs that dip gently and vary from a 2 m to ~ 10 m in amplitude. Zones of fractures are found along the upper limbs and rubbly toes at the base. Crests can be traced for over 1 km. B. Laterally discontinuous monoclines form densely fractured, often disintegrated blocks in the hanging wall of faults. Lengths vary from 10 m to 150 m and amplitudes from 2 m to 15 m. Solid red line in part A highlights monocline profile. Dashed blue lines: extent of continuous monocline; dashed orange line indicates extent of discontinuous monocline; dashed red lines: continuous open fracture; dashed yellow lines: extent of hanging wall buckles.

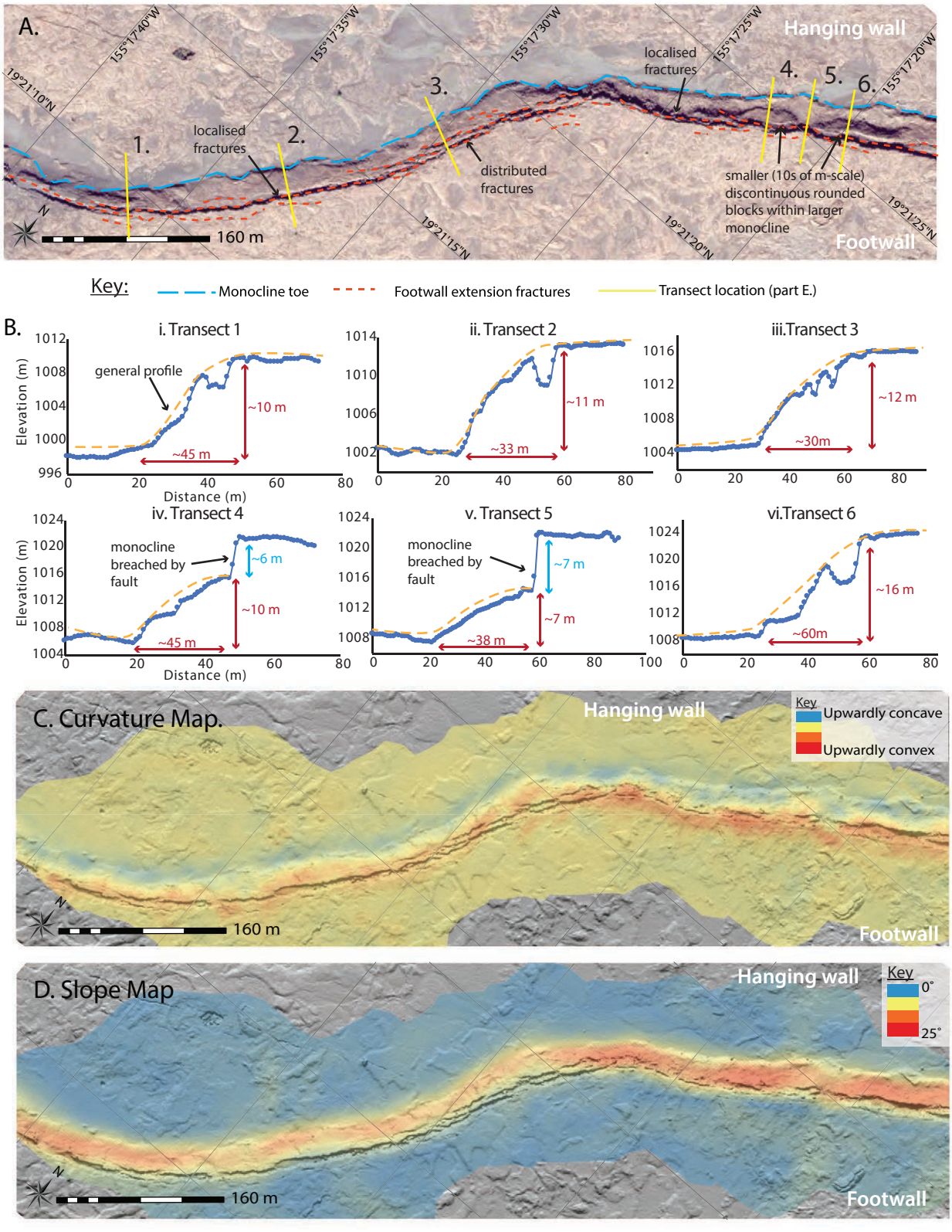

Figure 6. A. Map view of the continuous monocline shown in Figure 5, showing the distribution of extension fractures along the upper limb (dotted red lines). For location, please refer to the inset map for Figure 5. B. Cross-sections across the monocline in part A. Transect locations are show in part A. Transects 1-3 and 6 show steep, rounded monoclines with extension fractures along the region of maximum curvature. Transects 4 and 5 show a region of the monocline that has been breached by fault segments. The extent of this breaching is spatially limited. C: A map highlighting changes in 3D surface curvature across the monocline in part A. D. A slope map across the monocline in part A. Slope angles for the monocline limb range from ~12-25˚ with these values varying along-strike. Base image in A is an aerial World-View 2 satellite image (0.5 m resolution). Terrain data in parts C and D are derived from aerial LiDAR dataset (0.5 m resolution) provided by OpenTopography and generated in ArcGIS® software by Esri.

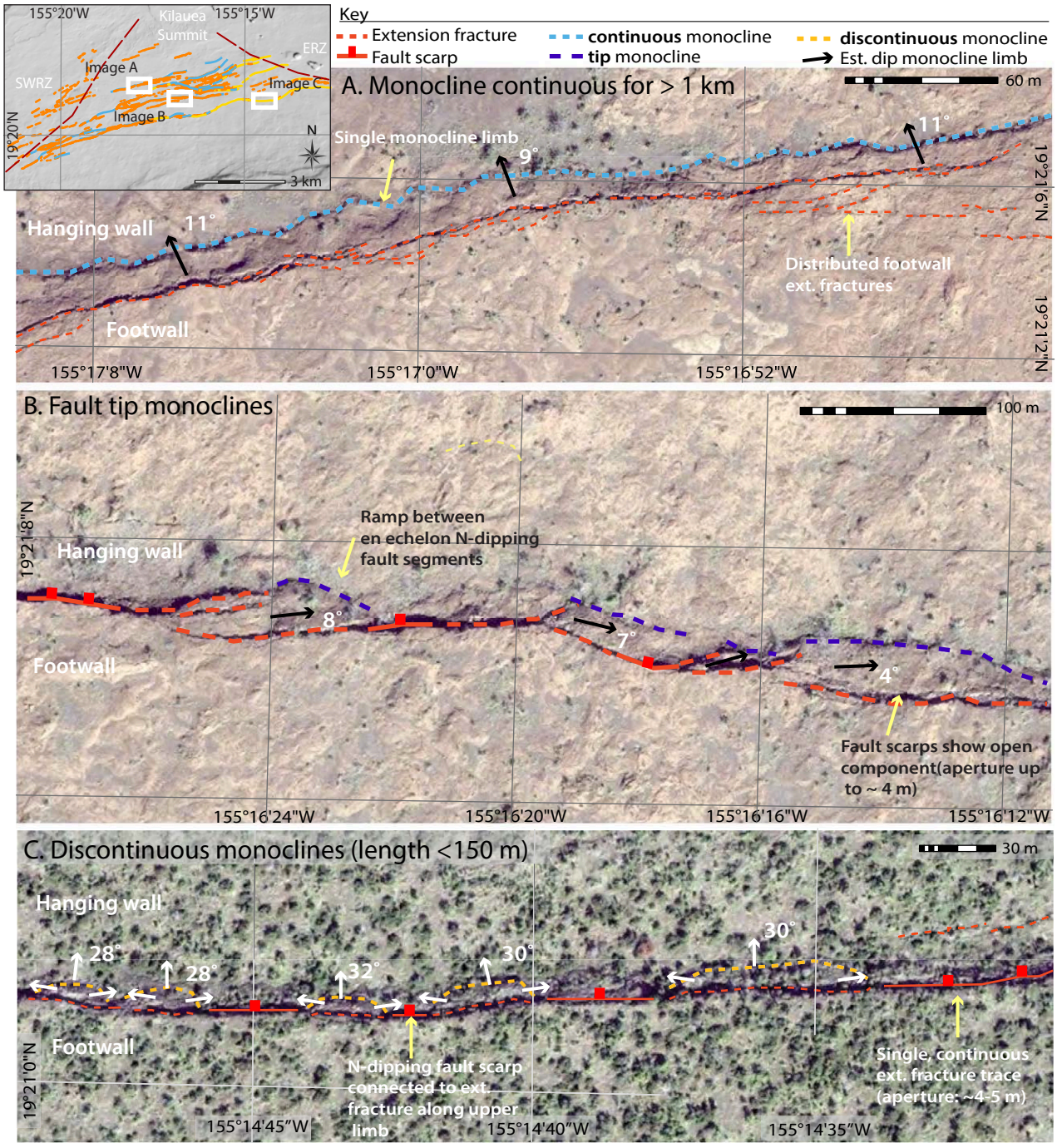

Figure 7. Map view of monocline types. A. Continuous monocline with a network of extension fractures along the upper limb. Limbs dip towards the north at ~10˚. Breached continuous monoclines are observed, but less commonly than unbreached. B. Fault tip monoclines between en echelon segments along the Ohale Fault. Tip monoclines dip parallel to the bounding segments by ~10˚. C. Discontinuous monocline blocks (dotted, yellow lines), isolated between normal fault segments (heavy red line), connected by collinear extension fractures (dotted red line) along the upper limb to form continuous open fractures that decouple the monocline from the footwall. These monoclines dip more steeply (~30˚) from a central amplitude maxima, to zero at the lateral edges. Breached discontinuous monoclines have not been observed. Base images: World-View 2 satellite image (0.5 m resolution).

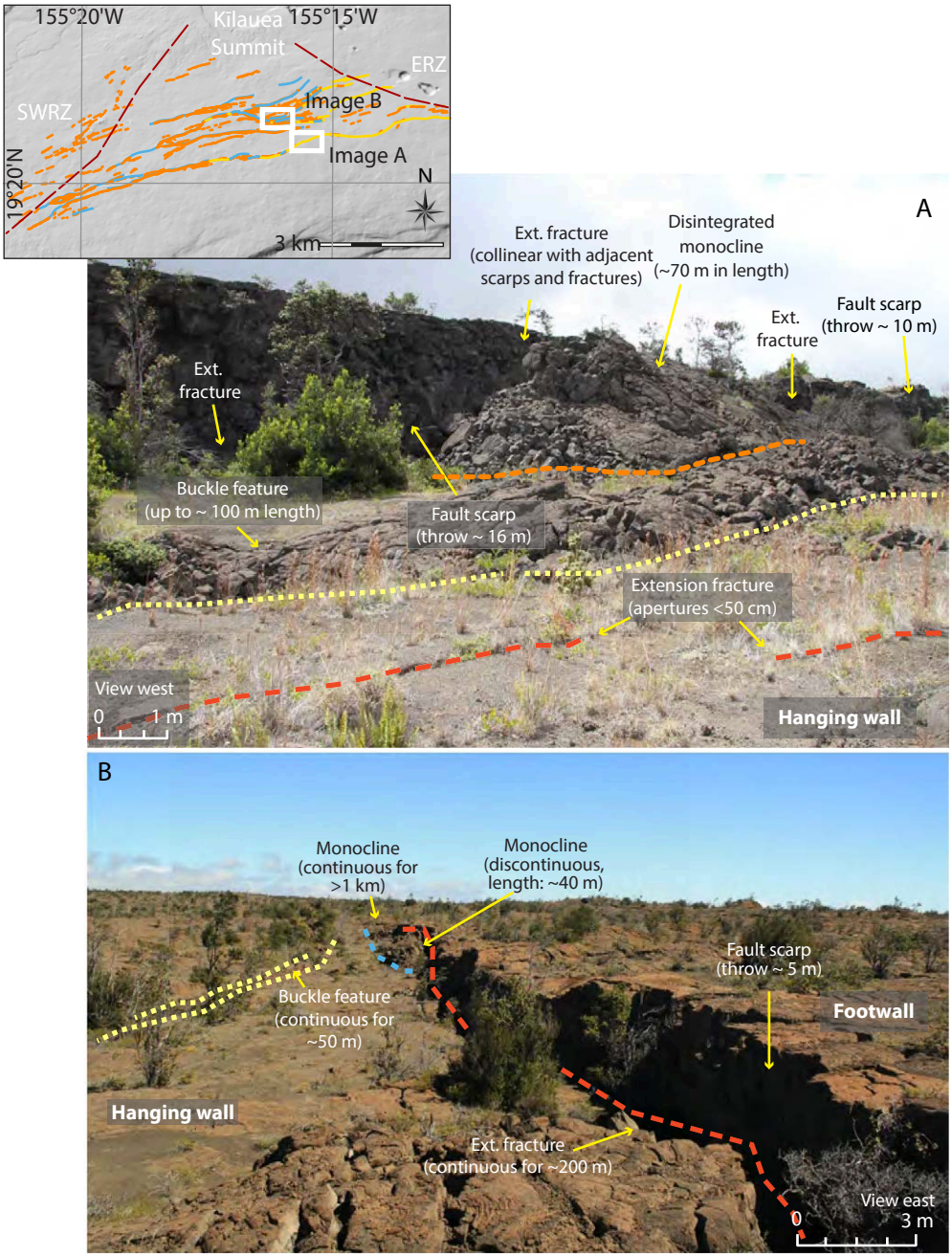

Figure 8. Examples of surface-breaking normal fault segments in the Koa'e fault system. Inset map indicates location for images in Part A and B. A. The largest vertical offsets (up to ~15m) and greatest proportion of fault scarps are found on the Kulanaokuaiki ("Shaking Spine") fault. B. Where present, scarps show a significant component of horizontal opening and offset planar footwall and hanging wall ground surfaces. Also present along many (but not all) faults in the Koa'e fault system are hanging wall buckles that occur ahead of both fault scarps and monoclinal structures. Dashed orange line: extent of discontinuous monocline; dashed blue lines: extent of continuous monocline; dashed red lines: continuous open fracture; dashed yellow lines: extent of hanging wall buckles.

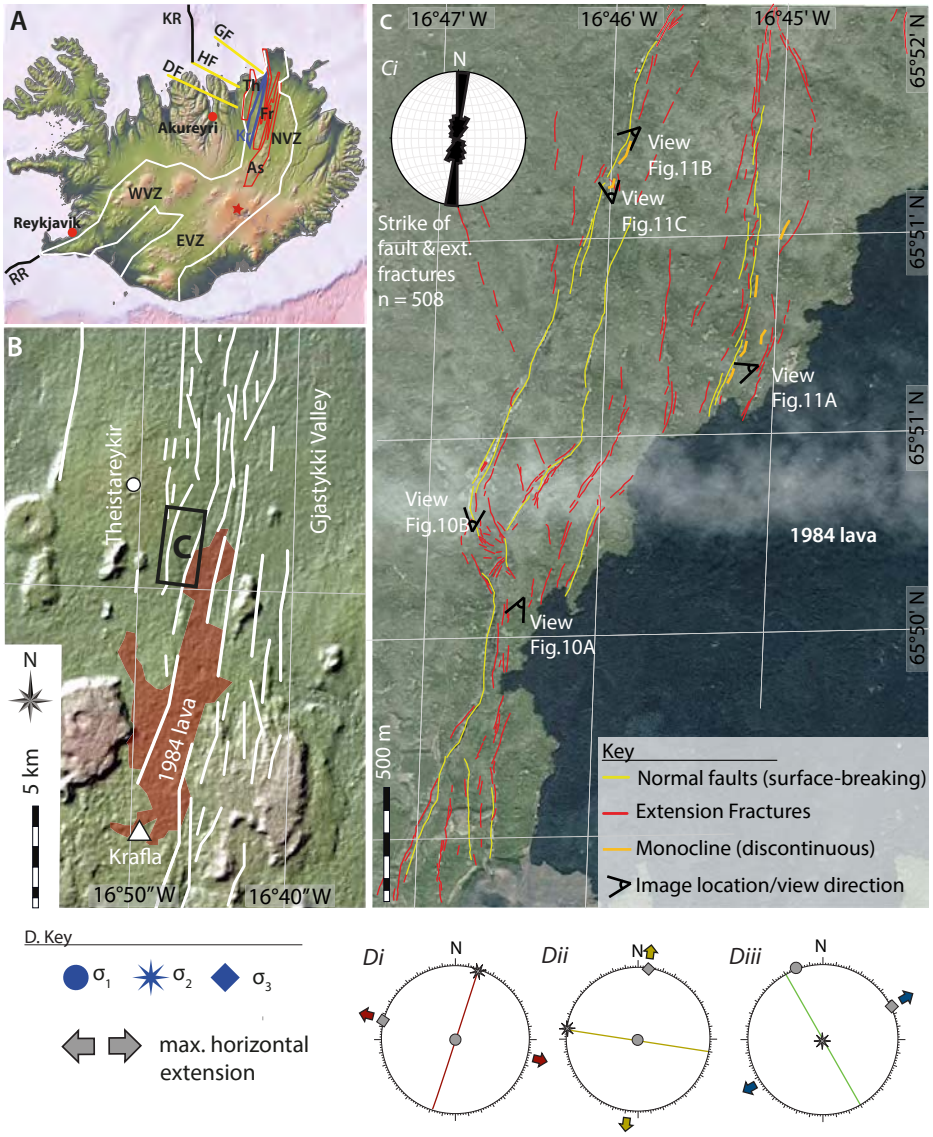

Figure 9. A. Map of Iceland highlighting the major tectonic elements: Reykjanes Ridge (RR); the Kolbeinsey Ridge (KR); West Volcanic Zone (WVZ); East Volcanic Zone (EVZ); Neo-Volcanic Zone (NVZ: the axial rift zone); Askja volcanic centre (As); Fremri-Namur volcanic centre (Fr); Krafla volcanic centre, (highlighted blue; Kr); Theistareykir volcanic centre (Th); the Dalvik lineament (DF), the Husavik-Flatey Fault (HF) and the Grimsey lineament (GF). B. Location of study area in the Gjastykki Valley within the Krafla fissure swarm. C. Mapped faults and extension/oblique-extensional fractures in the study area. Image locations and view directions in Figures 10 and 11 are indicated. C*i*. Rose diagram highlights the strike of normal faults and fractures in the Krafla fissure swarm. D. Lower hemisphere stereographic projections showing the average strike of fault/fractures and calculated maximum horizontal extension directions for the three dominant orientations: i) NNE-SSW striking faults and fractures, accommodating WNW-ESE extension; ii) WNW-ESE striking fractures, accommodating NNE-SSW extension; iii) NW-SE striking faults and fractures, accommodating ENE-WSW extension.

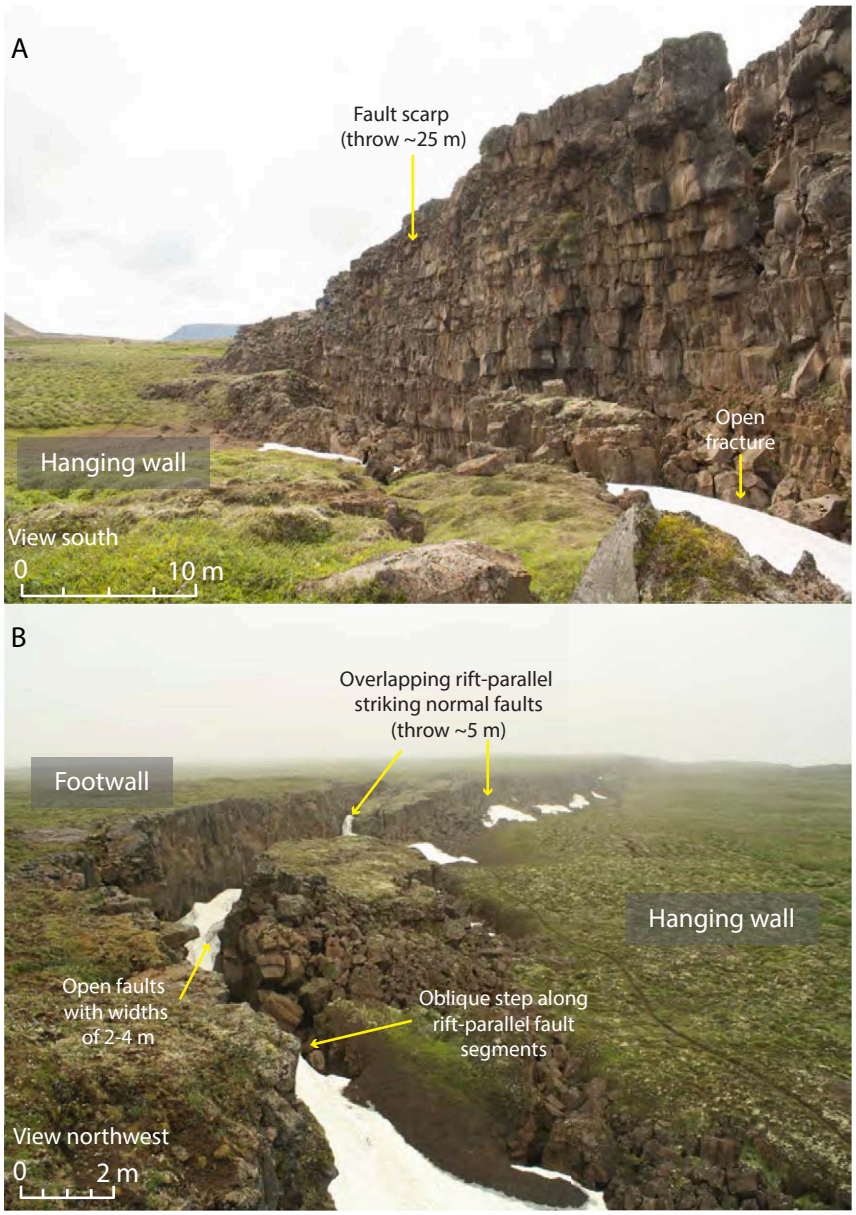

Figure 10. A. Examples of surface-breaking normal fault segments in the Gjastykki area of the Krafla fissure swarm. A. Subvertical normal faults demonstrate throws of up to 25-30 m and offset planar footwall and hanging wall surfaces. B. Rift faults show prominent horizontal openings of 2-4 m and overlapping geometries with obliquely-oriented linking segments. Inset map indicates the location of images in part A and B.

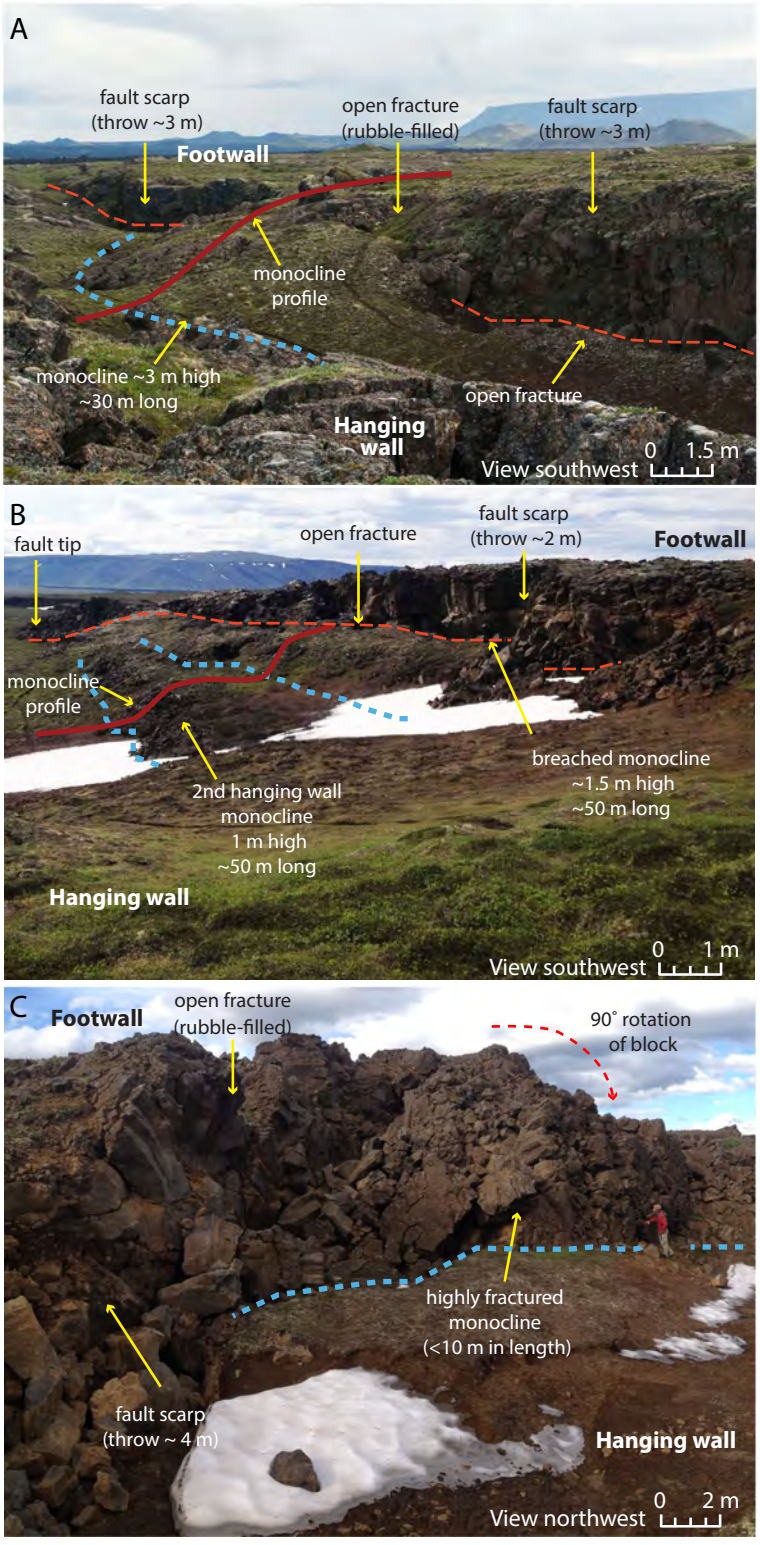

Figure 11. Examples of monoclines in the Krafla fissure swarm. A. Monoclines show amplitudes of up to ~3 m with open fractures along their upper limbs that are co-linear with fault segments on either side. B. Breached monocline observed in the hangingwall of a surface-breaking normal fault with vertical offset of up 2-3 m. Along the fault in the image, an additional monocline has developed further into the hangingwall. C. Monoclines can also be strongly fragmented and show steep rotations. In all examples, their lateral extent is <50 m.

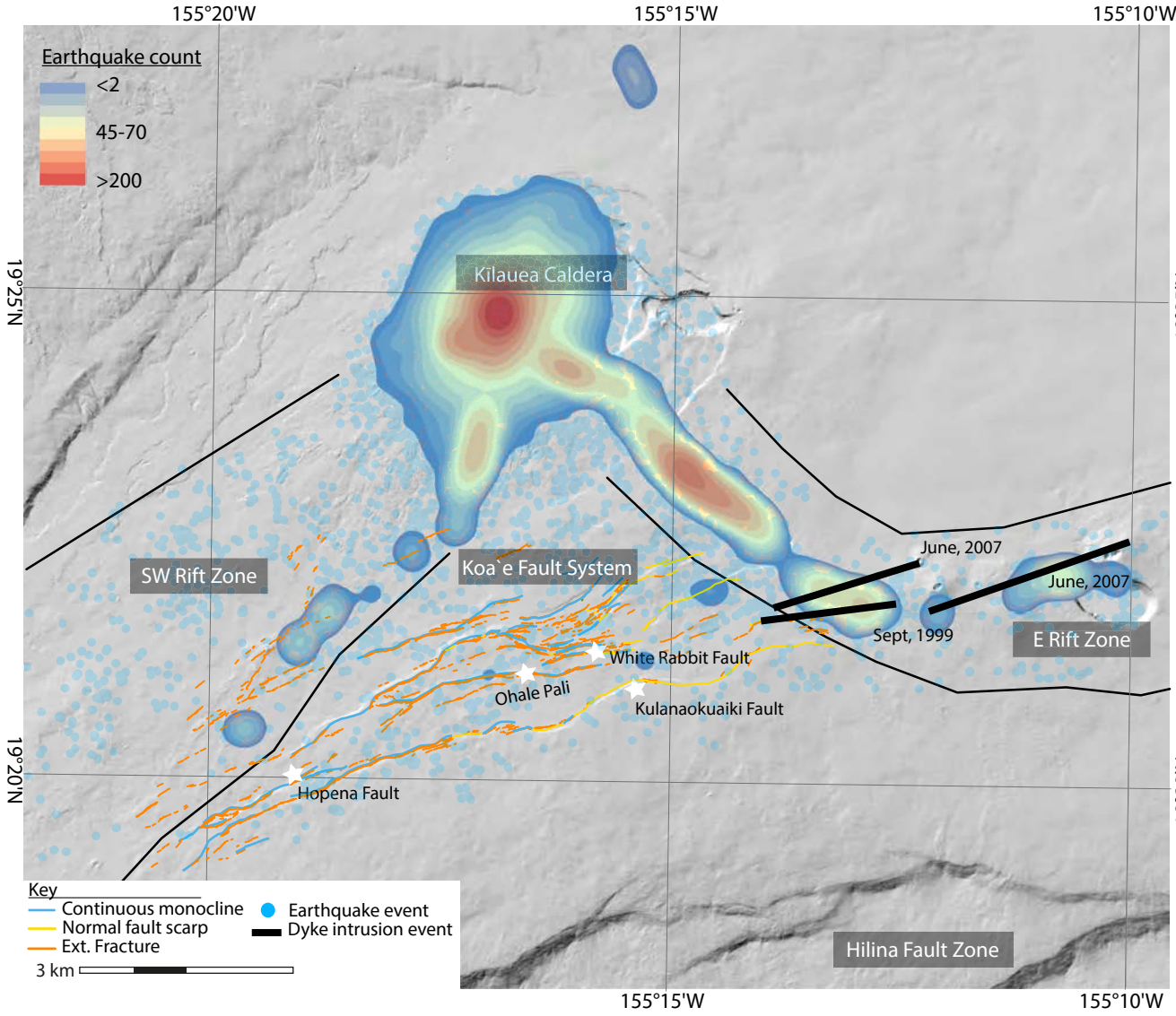

Figure 12. Distribution of surface-breaking normal faults and monoclinal folds across the Koa`e fault system. Blue circles represent focal mechanisms in the summit, upper ERZ and upper SWRZ regions of Kīlauea Volcano from the period 1986-2009. Contours highlight the density of events based on approx. 3000 focal mechanisms recorded in this region. Earthquake data reproduced from Lin and Okubo, 2016. ~90% of focal mechanisms in the catalog are small earthquakes (96% <M2.5), from shallow depths (i.e. <13 km); half of the focal mechanisms come from 2-5 km depth. Dyke intrusion events taken from Baker and Amelung, 2015 and Cervelli et al., 2002.

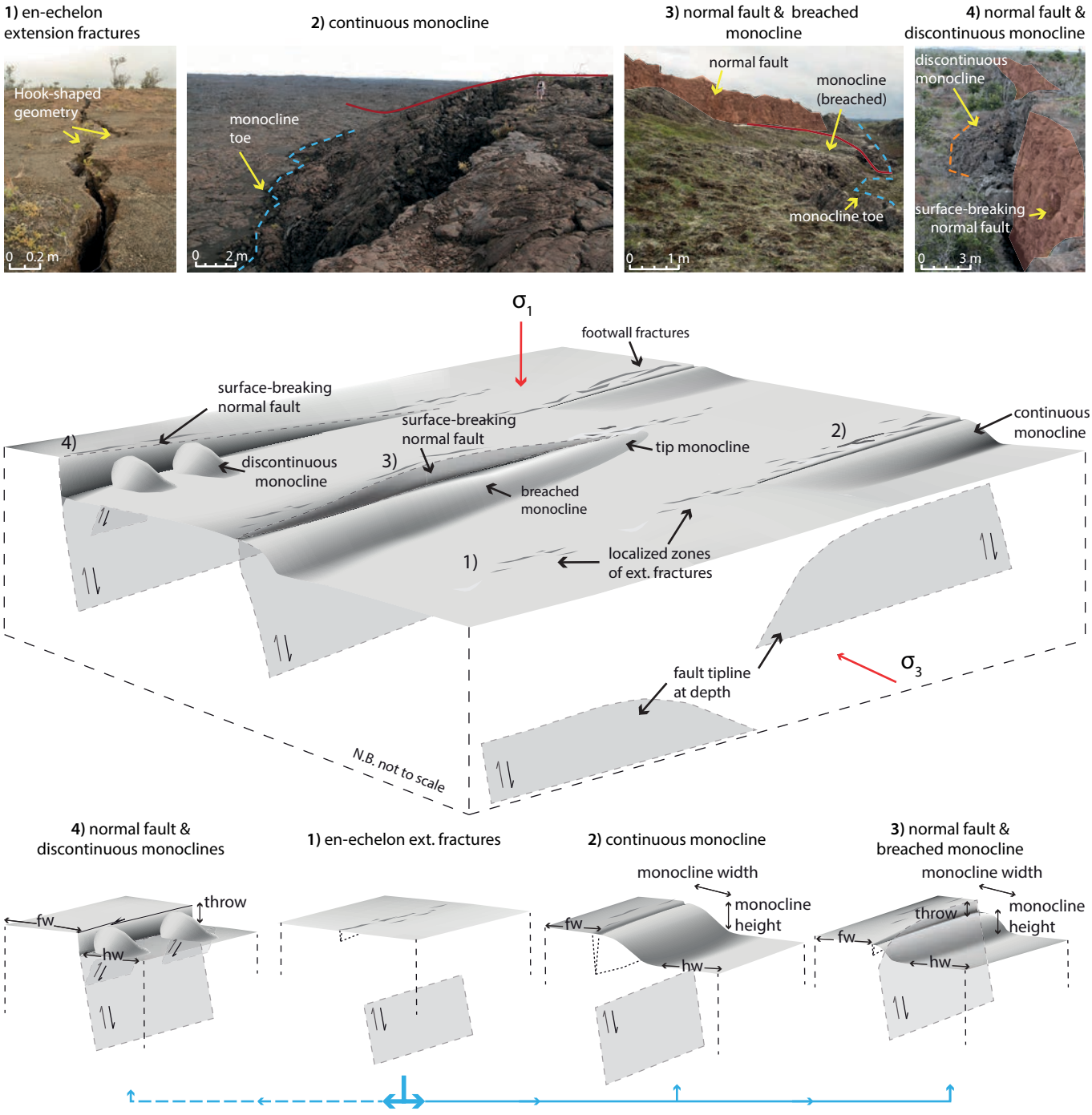

Figure 13. Conceptual model for growth faults in volcanic rift zones with spatially (and temporally) variable strain rates. Principal stress axes (red arrows) represent the regional stress state acting on the rift zone.
1. Precursory extension fractures localise in narrow zones at the free surface ahead of blind normal faults.
2. In regions of the rift zone where strain rates are low, faults remain at depth where they accumulate slip asesimically and gradually deform the free surface ahead of the tipline into monoclines.
3. In regions of the rift zone that experience episodically high strain rates, faults may spend protracted periods segmented at depth, followed by a rapid propagation phase that results in linkage with surface fractures and breaching of earlier formed monoclines at the free surface.
4. In regions of the rift zone where strain rates are high, normal faults propagate rapidly upwards through the sequence and link with downward propagating surface fractures, producing fault scarps. A lack of preserved monocline indicates strain rates have remained high since the last resurfacing event. Antithetic faults may develop from points of stress concentration, causing a rotation of the hanging wall block above them.